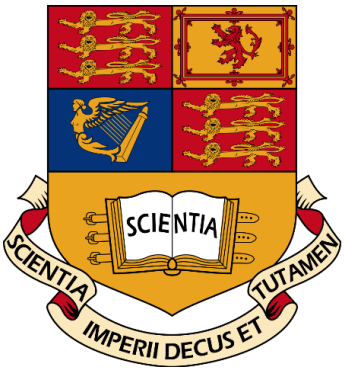

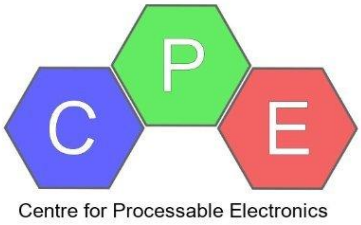

Photochemical Stability of Polymer Donors: PM6 and PTQ10

Author: Keren Ai

Supervisor: James R. Durrant

A thesis submitted in partial fulfilment of the requirements for the degree of Master of Research in Soft Electronic Materials

Department of Physics

Imperial College London

London, September 2022

Abstract:

The power conversion efficiencies of organic photovoltaics (OPVs) have reached ~20%, which is promising for commercialisation, driven by the fast development of non-fullerene electron acceptors (NFAs). However, the long-term stability of high-performance NFA-based devices is still a significant challenge. Previous research has already discussed the stability of NFAs, so this project aims to focus on donor material stability problems. Two efficient donor materials, PM6 and PTQ10, are employed in this study. Both of them perform high efficiency when blended with NFAs. We proved that PTQ10 has better photochemical stability than PM6 under combined exposure to simulated sunlight and oxygen. The light and oxygen exposure cause increased energy disorder in the PM6 domains, revealed by the vibronic peak loss in the absorption spectrum. Photoluminescence (PL) spectroscopy shows more nonradiative recombination in PM6 after oxygen exposure than light illumination, implying possible chemical reactions with molecular oxygen. There is no change in the ultrafast transient absorption spectrum of PM6 after the light soaking in nitrogen, while an exciton quenching and the formation of a polaron-pair state appear after light and oxygen exposure, which reduces the charge generation rate, causing degradation. Slow-TAS results attribute that the molecular oxygen reacts with PM6, which indicates an irreversible change in PM6 chemical structure. Thus, we reveal that the origin of degradations in PM6 may be oxygen-induced chemical reactions. Light exposure is possible to accelerate this degradation pathway and cause more severe degradation in the PM6 chemical structure. The crystallinity and molecular structure differences between PM6 and PTQ10 may contribute to photochemical stability differences. So far, PTQ10 has shown much better photochemical stability than widely used donor materials.

Acknowledgements

First of all, I would like to thank my supervisor Prof. James. Durrant for his expert and patient guidance. Special thanks to Dr Yiwen Wang and Dr Soyeong Jeong, who helped me patiently in this project. I am grateful to all durrant group members for their support. Thank you to my friends Jiaqi and Jiayi, also my classmates from the MRes Soft Electronic Materials course for accompanying me through this challenging year. The final acknowledgements must go to my parents for their selfless love and help.

Table of Contents

Chapter 1. Introduction

1.1 Photovoltaic Energy Development

As a result of the rapid development of both technology and the economy, the world's energy demand has dramatically increased. The primary energy sources are fossil fuels, including coal, natural gas, and petroleum. However, extraordinary mining and excessive use of fossil fuels has already led to catastrophic air pollution and global warming, which are severe challenges for humanity. Consequently, developing green and sustainable energy sources has become more critical. Solar energy is one of the most promising alternative energy sources. The amount of solar energy absorbed annually on Earth's surface (about 120,000 TW) is roughly 6-7 times more than global energy consumption[1]. Photon energy from the sun can be converted to electrical power via photovoltaic (PV) technology. According to the development history, PV cells are divided into three generations[2]. The first-generation system is mono- or multi-crystalline silicon with a p-n junction structure. The second generation is Cadmium telluride (CdTe) or copper indium gallium selenide/sulfide (CIGS) semiconductor-based photovoltaics. Both generations have excellent power conversion efficiency (PCE) of 26.1% and 23.4%, respectively[3], along with an extended lifespan (more than 20 years), so the first two generations have taken up most of the present commercial photovoltaic market. Meanwhile, the drawbacks of the first two generation photovoltaics are also apparent, such as higher production cost, fragility, and complex processing conditions[4,5], which cause insufficient compatibility in some application fields. The third-generation photovoltaics are developing now, which aim for better compatibility and properties. Organic photovoltaic (OPV) is one of the most promising third-generation solar cells, which uses organic materials to absorb photons and generate electricity. Compared with the first and second generation, OPV has low cost, solution processability, lightweight, semi-transparency and flexibility[5–7], which shows better potential in some application areas, such as the greenhouse, flexible electronics and indoor internet of things (IoT). In contrast, there are more difficulties for OPVs than inorganic PVs. The lower dielectric constant ($\varepsilon_\gamma \approx 2–4$) of organic semiconductors results in higher binding energy (≈ 0.3-1eV) of a bound exciton, representing a more considerable Coulombic barrier to separate electrons and holes[8,9]. Due to the localisation of charge states, organic materials have low charge mobility, which increases the possibility of charge recombination[10], limiting OPV device performance. So far, the commercialised silicon-based PVs have already reached >24% PCE and over 25 years lifetime[11,12]. Although the PCE of OPV is growing fast, the highest PCE reported (≈19%)[13,14] is still lower than silicon-based cells[13–15]. Meanwhile, there are a few reports focusing on the stability of OPVs. The stability of OPV is larging behind inorganic PVs as well[15,16]. To commercialise the OPVs, PCE and stability are still the main challenges to commercialise the OPVs.

1.2 Organic Photovoltaics History

The growth of OPV technology during the last few decades was remarkable. At the early stage, the OPV structure was designed based on a Schottky diode structure, which contains a single organic layer between the cathode and anode (Figure 1.1a), resulting in low efficiency[17–19]. In 1986, Tang et al. announced the first successful OPV based on the bilayer structure (Figure 1.1b). Copper phthalocyanine and a perylene tetracarboxylic derivative were used as the donor and acceptor layer, respectively, improving PCE to 1%[20]. The problem with the bilayer structure is that excitons, bound electron and hole pairs formed in the donor layer are too far from the donor/acceptor (D/A) interface. Since the lifespan only allows excitons to diffuse 5-14 nm[21–25], excitons have already decayed to the ground state before they reach the D/A interface. Therefore, the narrow charge production region at the D/A contact limits the efficiency of the bilayer OPV. In 1995, the bulk heterojunction (BHJ) OPV was designed to overcome this problem, and the reported devices achieved 2.9% PCE[26,27]. By controlling the phase separation between the donor and acceptor solutions in bulk, it can produce more extensive D/A interfaces in the heterojunction, which contributes a sufficient driving force to dissociate excitons and an efficient pathway for charge transport. In contrast, higher exciton disassociation efficiency and lower recombination loss result in better device performances. So far, the BHJ structure (Figure 1.1c) has become the most common structure of OPV devices.

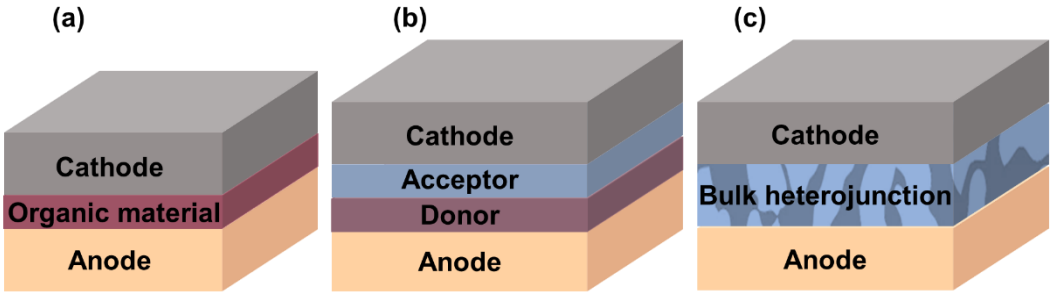

Figure 1.1. The OPV device overview of (a) a single layer structure (b) a bilayer structure (c) a bulk heterojunction (BHJ) structure[28].

1.3 Energy Conversion Mechanism

The BHJs commonly comprise a blend of an electron donating conjugated polymer and an electron accepting acceptor materials, forming the organic active layer to convert sunlight to electricity in the OPV device. The detailed energy conversion mechanism is illustrated in Figure 1.2.

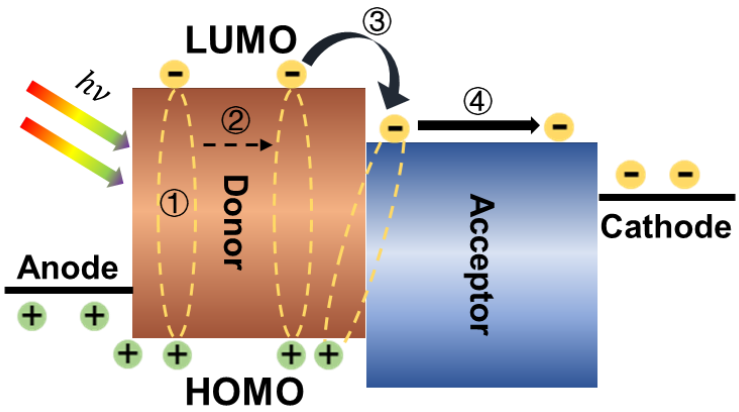

Figure 1.2. The OPV energy conversion mechanisms: 1) Exciton Generation. 2) Exciton Diffusion. 3) Exciton Dissociation. 4) Charge Collection[28].

Exciton Generation

Under light exposure, photons are absorbed by donor and acceptor materials in the active layer. When absorbed photon energy is greater than the bandgap of materials, electrons will be excited from the highest occupied molecular orbital (HOMO) to the lowest unoccupied molecular orbital (LUMO), forming a bound electron and hole pair, called an exciton. Given that the dielectric constant in organic semiconductors is high, the binding energy of the formed exciton is considerable (0.3-1eV)[9]. The strong coulombic interaction between electrons and holes leads that the photo-generated exciton cannot dissociate into free charges directly.

Exciton Diffusion

Following the tendency from a high exciton concentration to a low exciton concentration region, excitons will diffuse to the D/A interface[30]. As discussed before, in order to achieve an efficient OPV device, excitons should reach the D/A interface within their lifetime, which only allows excitons to diffuse 5-14 nm [22–26]. Exciton quenching and recombination at this process will lead to performance losses of OPV cells.

Exciton Dissociation

At the D/A interface, the electron transfers to the LUMO level of the acceptor, and the hole remains in the donor, which leads to the D+/A− condition, also called the charge transfer (CT) state. The rate of exciton dissociation is essential to achieving efficient OPV devices. Ideally, high charge separation efficiency, high charge transfer rate, and low recombination rate will significantly improve device performance.

Charge Collection

The energy offset between LUMO levels in donor and acceptor materials is the driving force, which moves disassociated electrons and holes along the internal electric field efficiently

to reach the two electrodes. Holes will reach the anode, and electrons will be collected by the cathode. The energy barrier between the anode and the HOMO level of the donor, along with the ohmic contact between the LUMO level of the acceptor are helpful for charge collection. The poor mobility of charges and recombination are the major losses in this process.

1.4 Photochemical Stability Challenge

The long-term stability is considered the main challenge for the commercialisation of OPV cells, especially photochemical stability. As reported, OPV devices without encapsulation degraded 80% of their initial PCEs after several hours or even minutes in the air[29]. Therefore, it is crucial to understand the origin of degradations for improving the designs of OPV. The primary origin of OPV degradation has been found as photooxidation under illumination in air, which is the concern of photochemical stability[30]. Oxygen and water can limit the performance of OPV, as Figure 1.3 states[31].

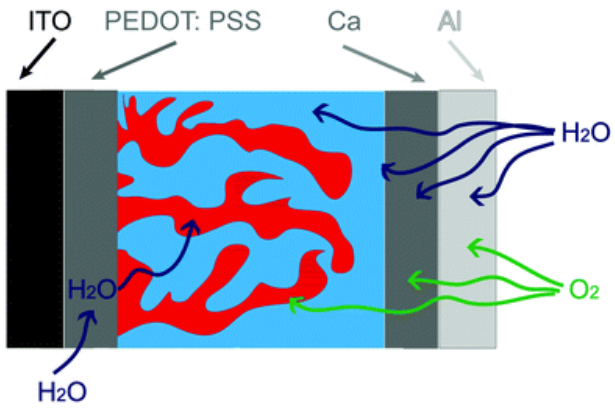

Figure 1.3. An overview of the oxygen and water diffusion in OPV devices [31].

First, the metal electrode with a low work function (such as Aluminium (Al) and Calcium (Ca) can form an electrically insulating metal oxide layer between the electrode and the active layer when oxidised by ingressive oxygen. This transport barrier layer leads to an S-shaped J-V curve and the reduced performances of OPV [32,33]. Also, the oxygen ingress of the active layer can cause multiple photooxidation processes of donor and accepter blends[34,35], resulting in changed chemical structures of materials. In this case, photon absorption, charge carrier mobilities and energy levels of donor and acceptor materials are influenced simultaneously. In addition, the doped oxygen molecules increase hole concentration in the active layer, which increases the density of traps for electrons. As a result, fill factor (FF), and open-circuit voltage (Voc) are reduced, which leads to a decay of the PCE performance. Furthermore, the impact of UV light on the OPV degradation mechanism has been discussed. Some researchers have already found that UV radiation can change the molecular[36,37] and microstructure[37] of BHJ layer materials, potentially

leading to defect/trap states and degradation. Another argument suggests that the leading cause of degraded device performance is the UV-induced degradation of the interlayer instead of the BHJ layer[38]. It has also been reported that UV light, considered as one of the leading causes of photooxidation[30], not only induces a direct degradation of photosensitive materials but also a generation of reactive oxygen species (ROSs)[39]. Nevertheless, visible light has been found that it can generate ROS in the photosensitive materials in OPV[40,41]. Two typical ROSs likely to induce photooxidation of organic materials are singlet oxygen and superoxide radicals.

1.4.1 Oxygen-induced Degradation Pathways

To present, two typical oxygen-induced degradation pathways have been reported: singlet oxygen generation and superoxide radical anions. The formation of singlet oxygen results from excited-state energy transfer from the triplet state of organic molecules to oxygen molecules, and the triplet state of the organic molecule must have higher energy than the singlet state of oxygen[42]. The triplet-mediated degradation mechanism has been explored in polymer donor systems (Figure 1.4)[43].

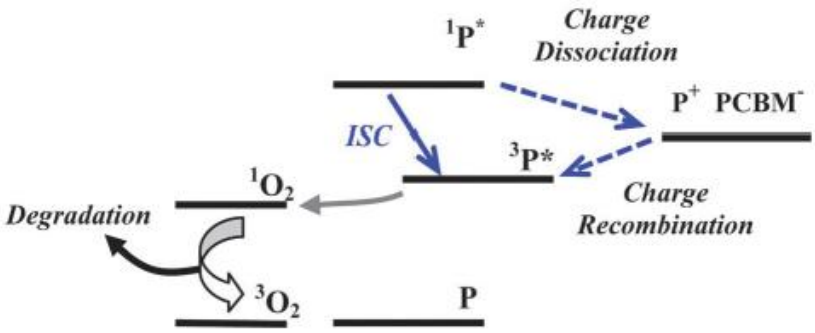

Figure1.4. The processes of triplet formation in neat and blend polymer films[43].

In neat donor films, triplets are formed via the intersystem crossing from polymer singlet state to triplet state (solid blue line). For blend systems, triplets are formed by charge recombination of dissociated polarons (blue dashed line). During the oxygen quenching process, energy transfers from the triplet state to molecular oxygen, generating singlet oxygen. The crystallinity of materials is also a determinant of triplet lifetime and oxygen quenching efficiency[44]. For more amorphous polymers, the triplet lifetime is longer, which gives triplets more time to interact with molecular oxygen. Therefore, their oxygen quenching rates are higher. The measurements of local oxygen concentration and diffusion in OPV devices have also been studied to achieve high photochemical stability. Many research focused on monitoring the phosphorescence quenching of added molecular phosphors to measure the oxygen concentration and diffusion within polymer films[45,46]. It turned out that the results were difficult to measure due to the potential interactions

between organic polymers and molecular phosphors. Fluorescence quenching investigations at high pressures have been used to study oxygen diffusion in semiconductor polymers[47,48]. Regarding the degradation mechanism, the singlet oxygen is created by the excited triplet-state energy transfer to oxygen molecules mentioned above[42]. It has been widely reported that the transient absorption spectroscopy technique is available to investigate the decay dynamics of triplet excitons in organic polymer/fullerene blend films and the oxygen-induced acceleration of decay dynamics[49–52].

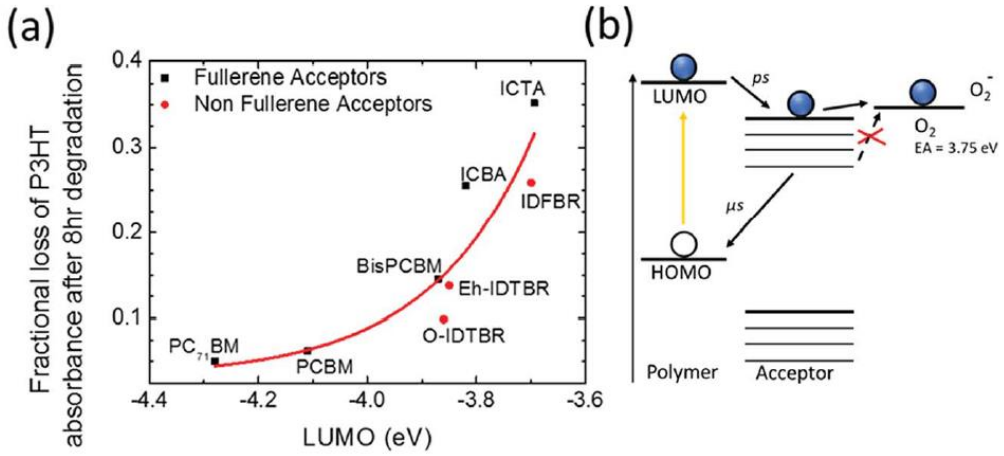

Figure 1.5: (a) Fractional loss of P3HT films after 8 hours AM1.5G light exposure respected with the changes of LUMO energy levels of acceptors[53]. (b) The proposed photodegradation mechanism of P3HT polymers and acceptors with superoxide formation[53].

When excited electrons transfer from organic materials to oxygen molecules, superoxide radicals are generated. The P3HT:FBR system photooxidation processes research discovered that the fast donor-acceptor charge transfer causes paltry triplet excited states for singlet oxygen generation[54]. However, the electrons of FBR transferred to oxygen molecules, triggering a greater generation rate of superoxide radical anions than that in the neat P3HT film[54]. Under the exposure of a fluorescent molecular probe, the formation of superoxide radicals has been investigated to be highly correlated to the LUMO levels of acceptors, disclosed by the transient absorption spectroscopy, as Figure 1.5(a) states[53]. The proposed photodegradation process of the P3HT film is demonstrated in Figure 1.5(b), which illustrates that a shallow LUMO acceptor level can facilitate the formation of superoxide anions, leading to further photochemical degradation[53]. In addition, electrons in the LUMO level come from the charge transfer from the HOMO level and leads to the possible photoexcitation of the acceptor, which is easier to happen in NFA systems because of their strong absorption. With regards to the above results, designing an active layer with a deeper LUMO energy level acceptor and a fast donor-acceptor charge transfer can reduce generations of singlet oxygen and superoxide radicals, improving the photochemical stability of OPV cells.

1.4.2 Challenges of Acceptors

Over the past 20 years, fullerenes and their derivatives have been widely used as electron acceptors and have contributed significantly to the development of OPV. Their delocalised lowest unoccupied molecular orbital (LUMO) electronic structure results in strong electron mobility. Meanwhile, 3D molecular structures of fullerene acceptors are suitable for the BHJ structure. Once blended with donor polymers, they can create efficient percolation, which is necessary for high-efficiency OPV devices[55–57]. However, the highly symmetric chemical structure and inadequate synthetic flexibility of fullerene materials resulted in weak photocurrent generation in the UV-visible range of the solar spectrum. Additionally, the energy levels of fullerene materials are difficult to change, so they cannot operate efficiently with different donors[58,59].

Small molecule non-fullerene acceptors (NFAs) have recently developed to overcome problems of fullerenes. With push-pull hybridisation, NFAs can reach broader absorption from the visible to near-infrared (NIR) range of the solar spectrum, contributing to efficient photon collection and better output current density[60]. The high synthetic flexibility of NFAs causes the tunable electron affinity and bandgap, which shows great potential for different application areas such as indoor PVs[61–63]. It has been proved that the radiative and non-radiative recombination losses are reduced in NFA-based OPV, which is beneficial for higher voltage output in device performances.

The fullerene acceptors have been well investigated those epoxides and carbonyl on the C60 cage formed due to photooxidation[64,65]. There are also a few reports on the photochemical stability of NFA. Considering ITIC as an example, it has been compared with fullerene $PC_{71}BM$. With different light exposure times, the colour of the ITIC film fades gradually, but $PC_{71}BM$ film almost remained its attenuation coefficient, as shown in Figure 1.6(a)[66]. ITIC's absorption peak was drastically reduced in intensity and experienced a blue shift after exposure compared to the $PC_{71}BM$ film, as Figure 1.6(b) indicates[66]. It has been observed that ITIC has more photo-oxidation reaction sites than $PC_{71}BM$, including the double bond between the donor and acceptor materials, the double bond on thiophene, or bithiophene outlying core building blocks, side chains, and so on (Figure 1.6(c))[66]. Exposure to air can cause irreversible reactions with molecular oxygen and the breakdown of molecular backbones at these active reaction sites. This will result in more trap states and energy loss, particularly in non-radiative recombination[66]. The PCEs of ITIC-based OPV devices (with J71) decreased to 70-100% initial PCEs after only 30-min light and air exposure with different device structures and interlayers[66]. As discussed, the photochemical instability of NFA-based cells is even more severe than that of fullerene-based cells. Moreover, encapsulation is a widely used method for avoiding oxygen and water ingress and providing mechanical protection for OPV devices to enhance photochemical stability[67]. For example, Sarkar et al. demonstrated that a thin Al_2O_3 film deposited by atom layer deposition (ALD), a standard encapsulating layer, can help a P3HT–PCBM cell remains 80% of its original PCE after 500 hours in the air[68]. Although

encapsulation is proven for improving device stability, its high fabrication cost is still a big concern for commercialisation. Therefore, improving the intrinsic stability of NFA is essential.

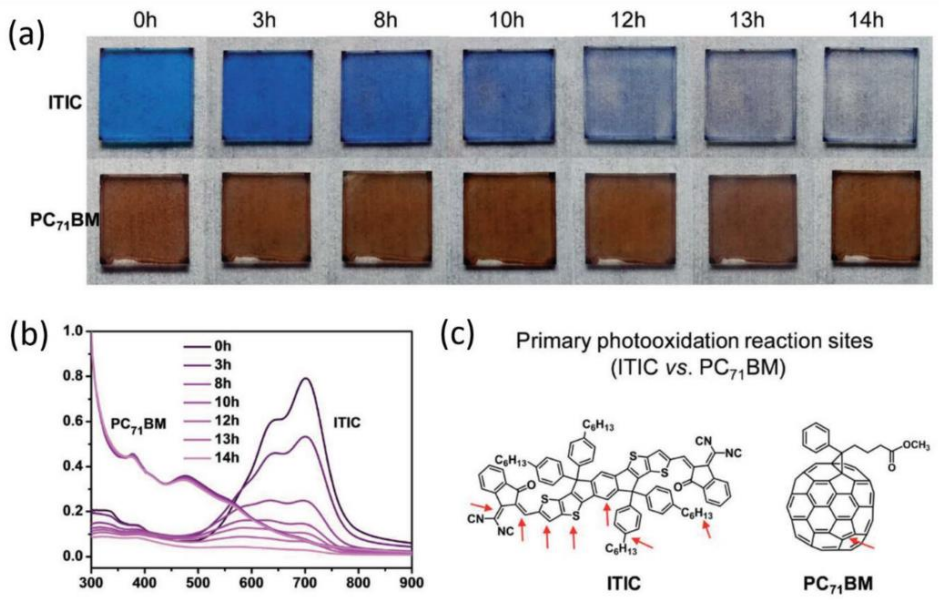

Figure 1.6: (a) Photos of ITIC and PC71BM films photo-bleaching progress at various exposure periods. (b) UV-visible spectra of ITIC and PC71BM films with different exposure durations. (c) ITIC and PC71BM's primary photo-oxidation reaction sites[66].

1.4.3 Improved stability of NFAs

The stability of NFA molecules has been claimed to be improved by alternating the molecular structure. Regarding end groups, NFAs with chlorine-substituted end groups show better stability than those with fluorine-substituted units in fused-ring electron acceptor (FREA). IDIC-4Cl, IDIC-4F, and IDIC, for example, have small respective optical density losses of 0.04%, 0.08 % and 0.4 % per hour[66]. On the other hand, the methyl-substituted end groups were less stable under light exposure[69]. Over the same illumination condition, ITIC-DM-based devices exhibit significant burn-in loss of short current density (J_{SC}) and FF, but ITIC-2F-based devices demonstrate potential long-term stability[69]. For ITIC-2F-based devices, the target of the remaining 80% of the original PCE is projected to reach after 11,000 hours, promising for developing photochemical stability[69]. Meanwhile, it has already been investigated that using non-fused donor cores successfully increases the stability of NFAs[70]. The Non-fused PTIC-based device is a good example, which can maintain 70% of its original PCE value after 50 hours of illumination. In contrast, under the same conditions, the fused ID-4F-based device only can remain just 25% of its initial PCE value[70]. The conformation of molecular structure is reported as an important role in NFA

photooxidation stability. For instance, the in-situ accelerated photoirradiation study of the materials Y6, ITIC, and O-IDTBR under a nitrogen environment revealed that molecular vibrational spectra of both IDTBR and ITIC changed significantly. In contrast, the vibrational spectra of Y6 showed no large changes. The excellent photochemical stability of Y6 is due to the alkyl side chain on the outer core, which serves as a conformation locker to prevent end-group rotation[71].

The improvements in stability of NFAs have been discussed above. Meanwhile, with the rapid development in the molecular design of NFAs, the efficiencies of OPVs have been improved dramatically, which already overtook the fullerene-based cells. The state-of-the-art single junction NFA-based solar cells have achieved ≈19% PCE[13], planar-mixed heterojunction solar cells achieved 19%[14] and tandem solar cells reached 20.2% PCE[72]. Such breakthroughs in the PCE indicate OPVs have great potential for commercialisation and are expected to be widely used in the short term.

Chapter 2. Motivation and Aims

Although the efficiency of OPV is increasing rapidly, many reports still indicate that OPV cells experience a fast degradation by photooxidation in the air. To prolong the lifetime of NFA-based OPV applications, it is necessary to enhance the photochemical stability of devices. Recently, there are improvements in photochemical stability of NFAs, as discussed in section 1.4.3. In contrast, there is a few related research on the photochemical stability of donor polymers. With the development of NFAs, a stable donor is also important to match with new NFAs.

Two wide bandgap polymer donors, PM6 and PTQ10, are employed in this project. Both donor materials achieve excellent efficiencies when blended with new NFA materials. Recently, PM6 has been blended with new NFA L8-BO (2-butyloctyl substitution), resulting in a surprising PCE of 19.2%[73]. For PTQ10, the best PCE so far is 18.55%, when blended with the new acceptor T2EH[74.] Since efficiency is already desirable, the long-term stability of high-efficiency solar cells become more critical for commercialisation. However, the PM6:Y6-based device (a record PCE of 15.7%[75]) shows poor stability. After 1 hour illuminance, its PCE decreased from 15% to 9%. It has been reported that the degradation in PM6:Y6-based devices mainly comes from the degradation of PM6[76]. On the other hand, the device of PTQ10:IDIC blend (~12.13%PCE) with simple encapsulation has good stability, in which case, its PCE remained 87.82% after 1000-hour storage in air atmospheres[77]. Therefore, this project aims to compare the photochemical stability of PM6 and PTQ10 neat donor films and to observe the possible degradation pathways.

Chapter 3. Experiments and Methodology

3.1 Materials

PM6 (also known as PBDB-TF, PBDB-T2F) is a D-A type copolymer based on 4,8-bis(5-(2-ethylhexyl)-4-fluorothiophen-2-yl)benzo[1,2-b:4,5-b']dithiophene (BDT-F) and 1,3-bis(thiophen-2-yl)-5,7-bis(2-ethylhexyl)benzo-[1,2-c:4,5-c']dithiophene-4,8-dione (BDD), synthesised in 2015[78] (Figure 3.1(a)).The bandgap of PM6 is around 1.8eV, with a deeper HOMO level ≈-5.5 eV which is helpful for high Voc as Figure 3.1(c) illustrates. PM6 used in this project is purchased from Solarmer.

Compared with PM6, PTQ10 is a relatively new donor material synthesised in 2018 (Figure 3.1(b)).[82]. The molecular design of PTQ10 [(thiophene)-alt-(6,7-difluoro-2-(2-hexyldecyloxy)quinoxaline)] is based on the D-A copolymerisation with simple thiophene ring D-unit and difluorine-quinoxaline A-unit. The raw materials required for PTQ10 are very cheap, and the synthesis only contains two steps with a high yield of 87.4%. PTQ10 has an optical bandgap of 2.7 eV, a HOMO level ≈-5.7 eV and a LUMO level ≈-2.96 eV (Figure 3.1(c)). PTQ10 was purchased from 1 material.

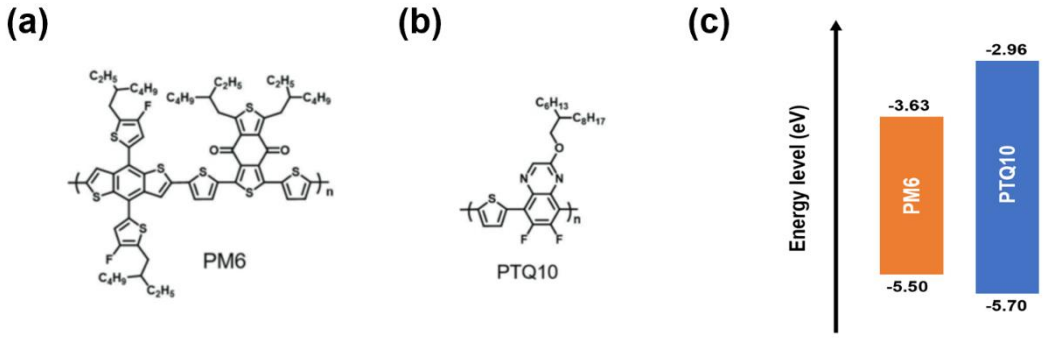

Figure 3.1. Chemical structure of (a) PM6 (b) PTQ10 and (c) energy level diagram.

3.2 Films Preparation

Neat PM6 and PTQ10 solutions were dissolved from chloroform at 8 mg/mL and stirred at 40 ℃ in the glovebox for at least 4 hours before use. All glass subtracts were cleaned in dilute detergent solution, deionised water, acetone, and isopropanol for 20 minutes with ultrasonication respectively, then dried by nitrogen stream followed by an oxygen plasma treatment. PM6 films were spin-coated on the glass subtracts in the glovebox at 3500 rpm

for 45 seconds. PTQ10 were spin-coated at 2500 rpm for 45 seconds at the same condition. All films are annealed at 100 ℃ for 10 minutes.

Ageing Conditions

There are three ageing conditions: Dark-O_2, Light-N_2, and Light-O_2. For Dark-O_2 treatment, films are immersed in pure oxygen flows for 2 hours under room temperature and dark conditions. The xenon lamp solar simulator with AM1.5 illumination of 100 mW/cm^2 is used for both Light-N_2 and Light-O_2 conditions. Films are treated for 2-hour light soaking under nitrogen and oxygen atmosphere at room temperature. As UV light has been reported as the main degradation origin for the active layer [36,37], to explore the photochemical stability impactors, UV light is blocked from illumination by UV filters.

Encapsulation

Encapsulation glasses were cleaned with the same procedure as subtracts. The films were encapsulated by epoxy glue with the encapsulation glass on top and then placed under a white lamp for 5 minutes.

3.3 Ultraviolet-visible Absorption Spectroscopy

Ultraviolet-visible (UV-vis) absorption spectroscopy is the fundamental technique to measure the amount of light absorption by materials at different wavelengths. When light travels through materials, the absorption energy enables electrons to move from the ground state (GS) to the excited state (ES). The *Equation* (1) is used to calculate absorbance by measuring the difference in transmitted light intensity with and without the sample:

$$\mathrm{A}(\lambda) = -\log \mathrm{T}(\lambda) = -\log \frac{\mathrm{I}(\lambda)}{\mathrm{I}_0(\lambda)} \tag{1}$$

where $A(\lambda)$= the absorbance at wavelength, $\mathrm{T}(\lambda)$= the transmittance at wavelength, $I(\lambda)$= light intensity transmitted, and $I_0(\lambda)$= light intensity received.

The absorption spectra were obtained by a spectrophotometer (UV-2600, Shimadzu) with a 1 nm interval step. It has integrated spheres (ISR-2600, Shimadzu) and a photomultiplier (PMT) tube R928 detector, enabling measurements across the electromagnetic spectrum using a "double beam - single detector arrangement" between 300 nm and 1100 nm. The UVProbe programme was used to measure the absorption spectra in a typical S/R (sample/reference) mode. The baseline was adjusted with a pristine glass substrate. Regarding the bandgap of PM6 and PTQ10, all measurements are from 300 nm to 1000

nm. Unencapsulated films with four conditions (Fresh, Dark-O_2, Light-N_2, Light-O_2) are employed in this characterisation.

3.4 Femtosecond Transient Absorption Spectroscopy (fs-TAS)

In order to measure the transient absorption (TA) spectra and kinetics of PM6 and PTQ10 neat films, a commercialised femtosecond (fs) transient absorption spectrometer called Helios (Spectra Physics, Newport Corp.) was utilised in this project. A 1 kHz Ti:sapphire regenerative amplifier was used to produce ultrafast laser pulses (800 nm, 100 fs pulse duration) (Solstice, Spectra Physics, Newport corp.) Each pulse is split into a pump pulse and a probe pulse using a semi-transparent mirror after the Solstice amplifier. The excitation wavelength can be tuned in the 290nm-NIR region by directing the pump pulse to an optical parametric amplifier (TOPAS Prime, Light Conversion) and a frequency mixer (NirUVis, Light Conversion). The timing at which the sample is probed is determined by passing the probe pulse through a delay stage that delays it relative to its corresponding pump pulse. The maximum duration of the delay stage in this system is ~6 ns. After the delay step (still 800 nm pulse), the probe pulse is focused into a sapphire crystal, which uses self-phase modulation to convert the monochromatic beam into a continuous white light. The resulting continuum enables the wide wavelength probe range; depending on the sapphire crystal thickness inserted, either a visible probe continuum (450–800 nm) or a NIR probe continuum (850–1400 nm) can be produced. In order to account for variations and boost the signal-to-noise ratio, the generated continuum pulses are then separated again using a semi-transparent mirror, with one probing into the sample and the other acting as a reference. A separate multichannel spectrometer (Si or InGaAs) is eventually focused onto each of the two continuum pulses. The pump pulse on the sample then spatially overlaps with the continuum pulse that probes through the sample. By blocking the pump pulse with an optical chopper revolving at 500 Hz, it is possible to monitor the absorbance in the excited state and the absorbance in the ground state for the calculation of the absorbance difference ΔA. The entire set-up of this equipment is illustrated in Figure 3.2. With a pinhole of 500 μm in diameter, the energy metre (VEGA P/N 7Z01560, OPHIR Photonics) was used to measure the pulse energies. Samples were kept in a quartz cuvette for the measurements under a constant nitrogen flow. The measured spectra were averaged over numerous scans to provide a reasonable signal-to-noise ratio and normalised to the reference spectrum to account for fluctuations. All collected TA results were corrected by Surface Xplorer's built-in functions, which include background noise and scattering light subtraction, chirp correction, and "time-zero" correction. According to the UV-vis spectra of PM6 and PTQ10, the excitation wavelength 580 nm was chosen for fs-TAS measurements of the two materials.

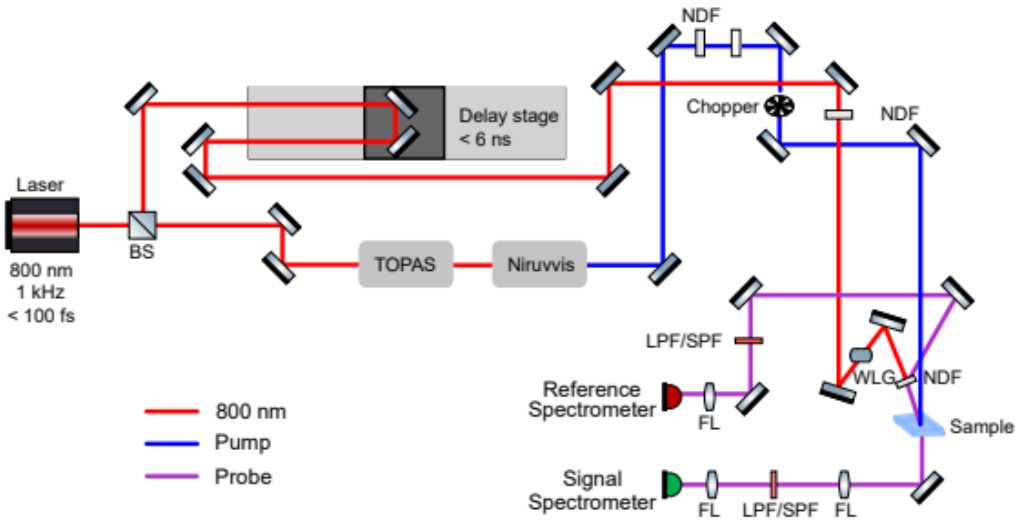

Figure 3.2. The detailed layout of the fs-TAS system, where BS is beam splitter, NDF is neutral density filter, LPF is long pass filter, SPF is short pass filter, WLG is the sapphire crystal, FL is focal lens[79].

3.4.1 TA Signals

Change in optical density (ΔOD)

The light intensity difference, transmitted through the sample with and without the pump pulse, determines the absorbance change (ΔA)or optical density change (ΔOD) in TA spectroscopy. The spectrometer records the transmittance change (ΔT) at each pump-probe delay time over the whole probe wavelength range. According to *Equation (2)*, ΔOD can be transferred to ΔT:

$$\Delta OD = OD_2 - OD_1 = -log\left(\frac{I_2}{I_0}\right) - \left[-log\left(\frac{I_1}{I_0}\right)\right] = -log\left(\frac{I_2}{I_1}\right) \quad (2)$$

where I_0 is the light intensity received, I_1 is the light intensity transmitted with pump pulse, I_2 is the light intensity transmitted without pump pulse. Given that the light intensity difference with and without pump pulse is small (~10^{-3}), *Equation (2)* can be approximated to:

$$\Delta OD = -log(1 + \frac{I_2 - I_1}{I_1}) = -log\,(1 + \frac{\Delta I}{I_1}) = -\frac{1}{2.3} \times ln\,(1 + \frac{\Delta I}{I_1}) \approx -\frac{1}{2.3} \times \frac{\Delta I}{I_0} \quad (3)$$

The optical density change (ΔOD) is proportional to the light intensity change, which is known as $\Delta T/T$[80].

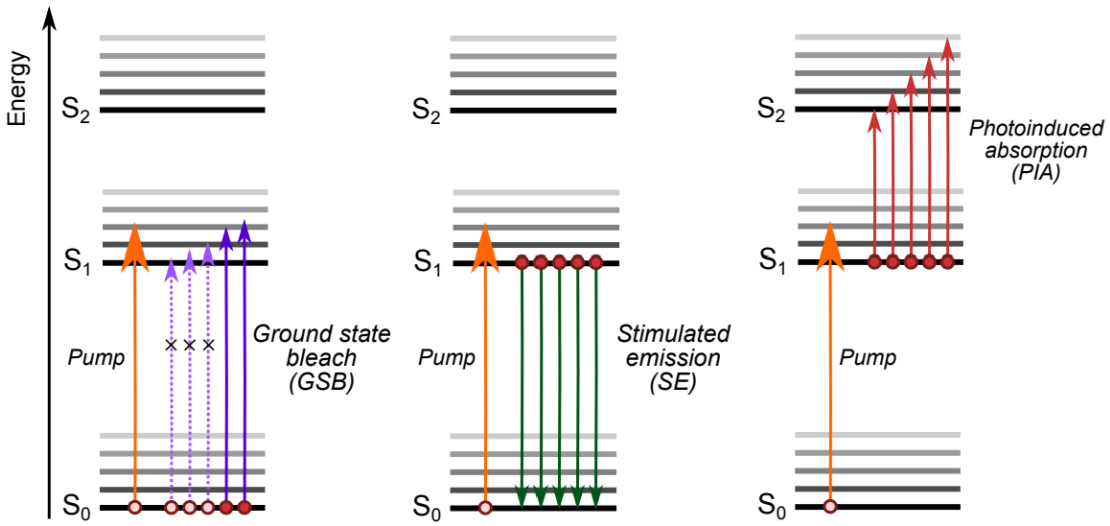

Figure 3.3. Energy level diagrams of ground state bleach (GSB), stimulated emission (SE) and photo-induced absorption (PIA)[79].

Ground State Bleach (GSB)

The population of ground state (GS) molecules decreases as the pump pulse promotes molecules from the ground state (GS) to the excited states (ES). Therefore, the excited sample has less GS absorption than the non-excited sample. This is depicted as a positive signal in the $\Delta T/T$ spectrum. The GSB signal can be recognised by comparing the UV-vis absorption and TA spectra.

Stimulated Emission (SE)

Following the population of excited-state species by the pump, SE represents the process where the photon from the probe pulse induces the emission of another photon from the excited state. This happens when the energy difference between the excited state and ground state is equal to the incident photon energy. With the pump pulse, the detector captures more light passing through the sample. Consequently, it appears as a positive signal on a $\Delta T/T$ plot.

Photoinduced absorption (PIA)

A portion of molecules are stimulated by the pump pulse, and excited-state species can participate in further optical transitions. As a result, a negative signal will appear in the $\Delta T/T$ plot. PIA signals in the organic semiconductors under study in this thesis commonly come from sources including excitons, charge-transfer states, and polarons.

3.5 Microsecond transient absorption spectroscopy (ms-TAS)

Similar with fs-TAS, micro-second transient absorption spectroscopy (ms-TAS) was employed to measure the optical density change with the delay time varied from microsecond to second, with a home-built ms-TAS set up (Figure 3.4). The 532 nm module of the laser (Nano S 120-20, Litron Lasers) was used as the pump pulse. A monochromator and a 100 W Bentham IL1 tungsten lamp serve as the probe light (OBB-2001, Photon Technology International). Another monochromator is tuned to the same wavelength as the probe beam to filter dispersed laser light. Using a Si-photodiode, the transmitted photons are detected (Hamamatsu). For the s-ms timescale, the collected data are processed using an amplifier from Costronics and then recorded using an oscilloscope from Tektronics (TDS 2012B), while the ms-s timescale data are recorded using a DAQ card (National Instruments, NI USB-6211). A LabVIEW program is designed to collect the data.

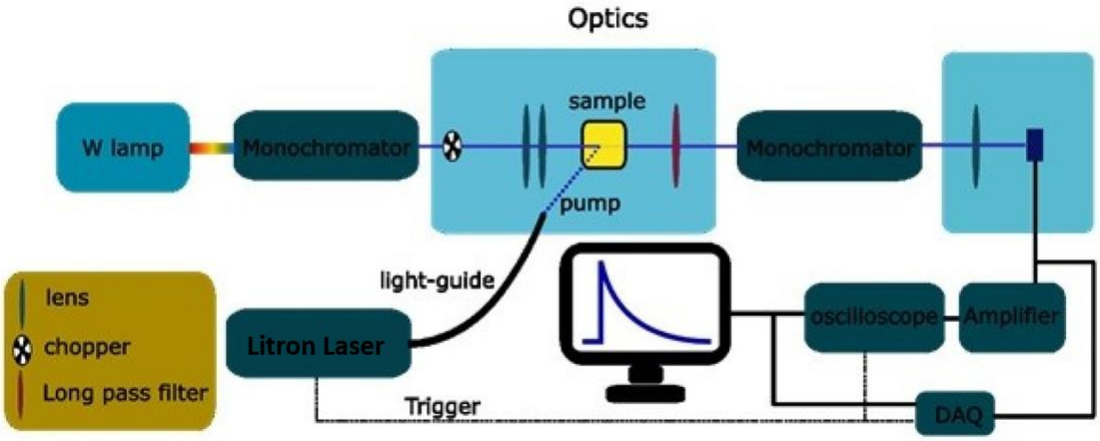

Figure 3.4. The set-up of ms-TAS system.

3.6 Photoluminescence (PL) spectroscopy

When the photons are absorbed, the material will be excited to a higher electronic state by the photoexcitation, and as it returns to its original lower energy level after relaxing, it will release energy (photons). Photoluminescence (PL) is the process of light or luminescence emission as the Jablonski diagram shows (Figure 3.5). When carriers decay from ES to GS, photoluminescence (PL) spectroscopy can measure the spontaneous emission of photons. The photons can emit randomly after being absorbed at a specific wavelength in the sample, producing a PL spectrum where the photon counts are displayed

as a function of wavelength. The energy of emitted photons is related to the difference between the orbitals or bands.

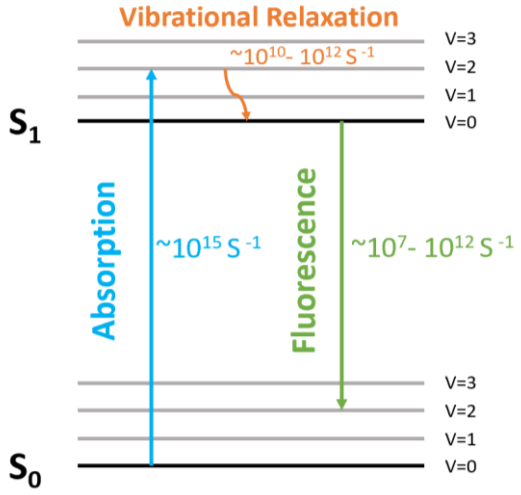

Figure 3.5. The Jablonski diagram shows the process of fluorescence emission.

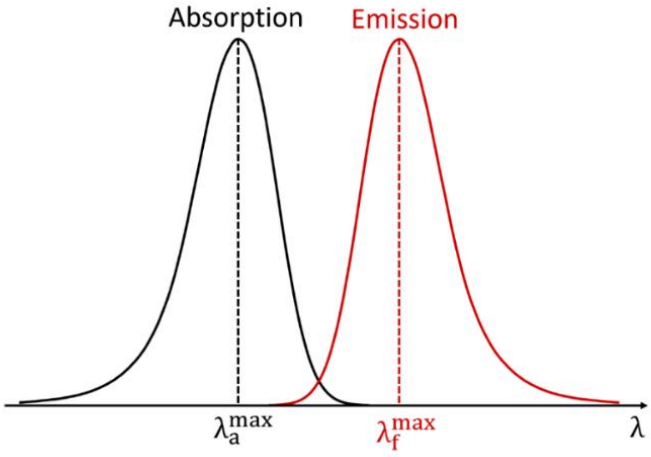

Figure 3.6. The Stokes shift between absorption and emission spectrum maxima[81].

The Stokes shift is the difference between the absorption and the emission spectrum maxima (Figure 3.6), which attributes from the rapid non-radiative decay to the vibrational ground state of the S1, after the initial excitation to the higher vibrational level of the S1 (Figure 3.5), resulting in a longer wavelength for the fluorescence since it has less energy than the absorbed photon. This explains the common red-shift peaks between UV-vis absorption and PL emission spectra. PL spectroscopy can also calculate the HOMO-LUMO gap in molecules or the direct band gap of semiconductors [82–84]. PL is frequently detected at photon energies below the band gap in semiconductors because defects often produce states in the band gap. The radiative and non-radiative recombination rates in material directly affect how

much photoluminescence will be. A FLS1000 photoluminescence spectrometer from Edinburgh Instruments was used for PL measurements. As the excitation light source, a pulsed laser diode with a wavelength of 532 nm was employed. Using an LED power metre, the fluence was measured for 532 nm at a frequency of 2 MHz, which was 45 mW/cm^2. The 590 nm long pass filter was placed before the detector to filter the reflected laser light. All samples for PL measurements were encapsulated to prevent the possibility of fast degradation during the measurements.

Chapter 4. Results

4.1 PM6

4.1.1 UV-vis Spectroscopy

To study the degradation mechanisms of PM6 neat film, UV-vis spectroscopy was utilised to observe the absorption spectrum. Figure 4.1 compares the absorption spectrum of fresh PM6 films and aged films. For fresh PM6 films, two absorption bands are shown from 300 nm to 700 nm, a common spectrum for D–A copolymers[78]. The absorption maximum is ~ 619 nm in the fresh PM6 film, and a prominent shoulder peak at ~580 nm is also seen. This shape represents the vibronic structure[85]. The PM6 film's absorption edge is at 690 nm, equivalent to an optical bandgap of 1.80 eV. As we can see, the absorption spectrums of Dark-O2 and Light-N2 samples have negligible differences from the spectrum of Fresh PM6 samples, which indicates that only light or oxygen exposure has a small impact on PM6 absorption. In contrast, the absorption spectrum of Light-O_2 film has significant changes. Firstly, there is a slight decrease in the ~312 nm peak. Then, it is striking that the maximum absorption peak ~619 nm is much lower than the one of fresh PM6 and the shoulder peak of 580 nm disappeared, indicating the vibronic structure is broken. Given that high-level ordering between the polymer chains is related to clear vibronic peaks in the absorption spectrum[86], the loss of vibronic peaks in the Light-O_2 film may be due to the increased energy disorder in PM6 domains which can be further proved by using photothermal defection spectroscopy. Moreover, the absorption edge becomes broader, which is ~750 nm for the Light-O_2 PM6 film, suggesting the band gap of PM6 decreased under the combined impact of light and oxygen. Based on the UV-vis absorption spectra, the absorption has a negligible change in only light or oxygen conditions. PM6 only shows a severe degradation under combined exposure to light and oxygen, which indicates the poor photochemical stability.

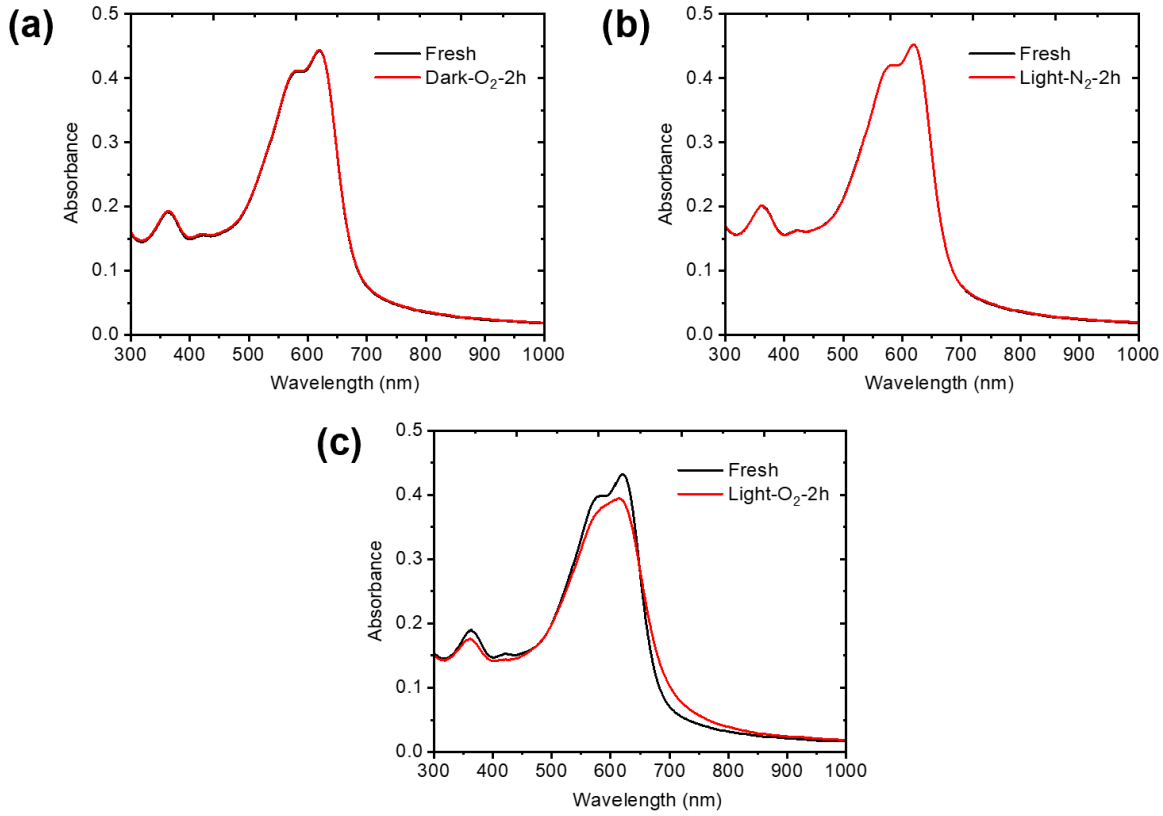

Figure 4.1. The UV-vis spectrum of Fresh, (a) Dark-O_2, (b) Light-N_2, (c) Light-O_2 PM6 films under the simulated sunlight (without UV light) and oxygen atmosphere for 2 hours.

4.1.2 PL Spectroscopy

It has been reported that PL spectroscopy is more sensitive than UV-vis measurements[87]. The PL spectrums were measured for PM6 films of four conditions with 532 nm excitation wavelength and 45 mW/cm^2 laser intensity. As shown in Figure 4.2, the PL spectrum of fresh PM6 film indicates a band peak of ~697 nm, attributed to the band-to-band transition in PM6 polymer. Compared with the absorption peak ~619 nm, there is a red shift between the absorption and emission spectrum maxima, which is assigned for the Stokes shift, which is explained in section 3.6. The PL spectra comparisons of ageing conditions are indicated in Figure 4.3. The PL spectra remain the same for Fresh, Dark-O_2 and Light-O_2 films, only peak intensity changes. The PL intensity relationship is Fresh > Light-N_2 > Dark-O_2. The quench of PL intensity means less fluorescence emission, suggesting more non-radiative recombination in the sample. Compared with the Fresh film, the Dark-O_2 film has more PL quenching than the Light-N_2 film, which means oxygen has more effects on PM6 degradation. It is also noticeable that the PL spectrum of Light-O_2 film is disappeared under the combined exposure to light and oxygen for only two hours, causing severe degradation in PM6, which possibly allocates that the chemical structure of PM6 polymer is broken during the ageing process. The possible degradation pathway is chemical reaction between

molecular oxygen and PM6. The light exposure may accelerate this degradation pathway and cause more severe degradation of the PM6 chemical structure.

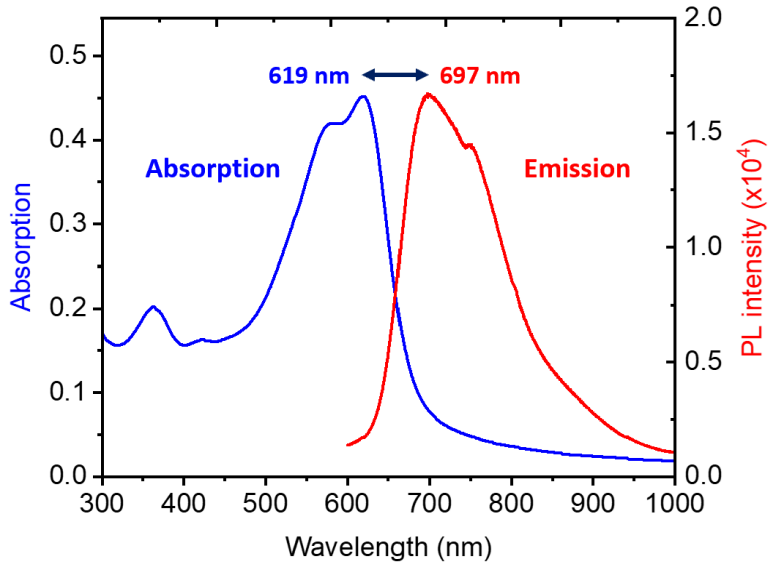

Figure 4.2. The Stokes shift between the UV-vis absorption and PL emission spectrums of fresh neat PM6 film, excited at 532 nm with intensity of 45 mW/cm^2.

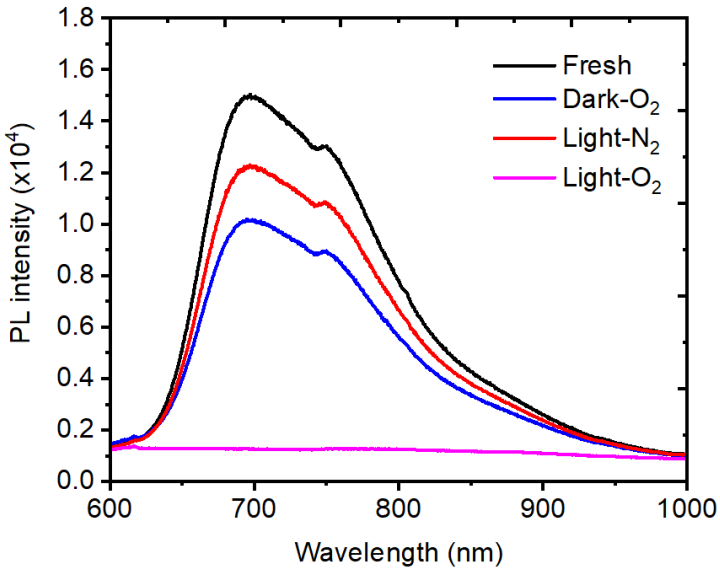

Figure 4.3. The PL spectrum of Fresh, Dark-O2, Light-N2, and Light-O2 PM6 films (two-hour ageing time), excited at 532 nm with the intensity of 45 mW/cm^2.

4.1.3 Fs-TAS

To further understand the degradation process of PM6 films, fs-TAS was used to measure fresh and aged films. The fs-TAS spectra of PM6 neat films under four conditions are shown in Figure 4.4, with a low fluence of 7.13μJ/cm^2 at 580 nm. First, we can look at the Fresh PM6 spectrum (Figure 4.4(a)). The ground state bleach (GSB) ranges from 500 nm to 700 nm with a peak at 630 nm, which reveals the photo-induced absorption from singlet excitons. A weak stimulated emission (SE) is around 700-750 nm, indicating the emissive nature of the intrachain excitons. The photoinduced absorption (PIA) is broader than the GSB in the near-infrared (NIR) region, where the peak is 1150 nm. The PIA signal appears right after the laser excitation (~0.2 picoseconds (ps)), which can be assigned to the formation of a PM6 singlet exciton S1. Compared with the Fresh sample, the Light-N2 film has a similar fs-TAS spectrum (Figure 4.4(c)).

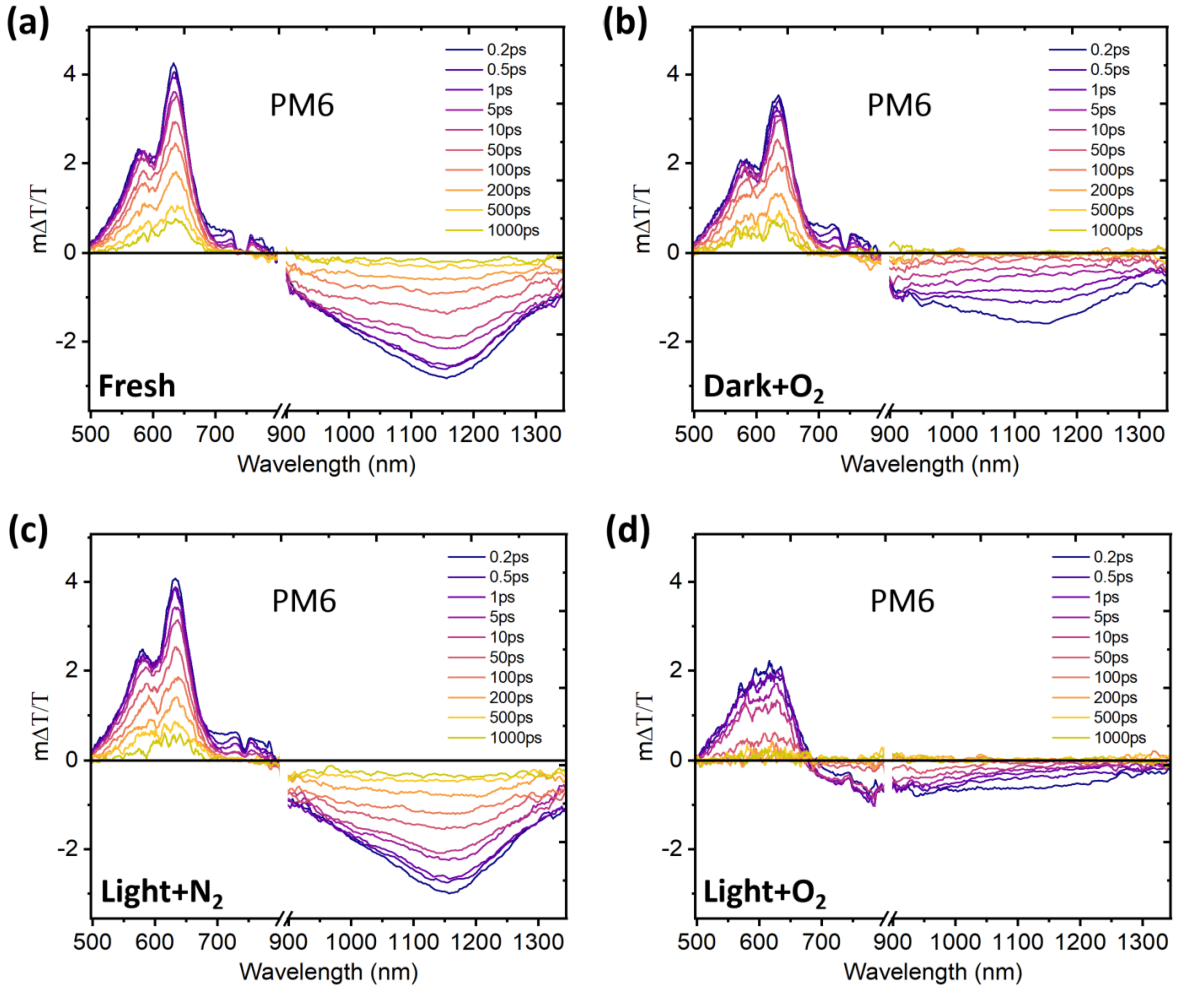

Figure 4.4. The fs-TAS spectrums of the (a) Fresh, (b) Dark-O2, (c) Light-N2, (d) Light-O2 PM6 films (two-hour ageing time), excited at 580 nm with the intensity of 7.13μJ/cm^2 under room temperature 298K.

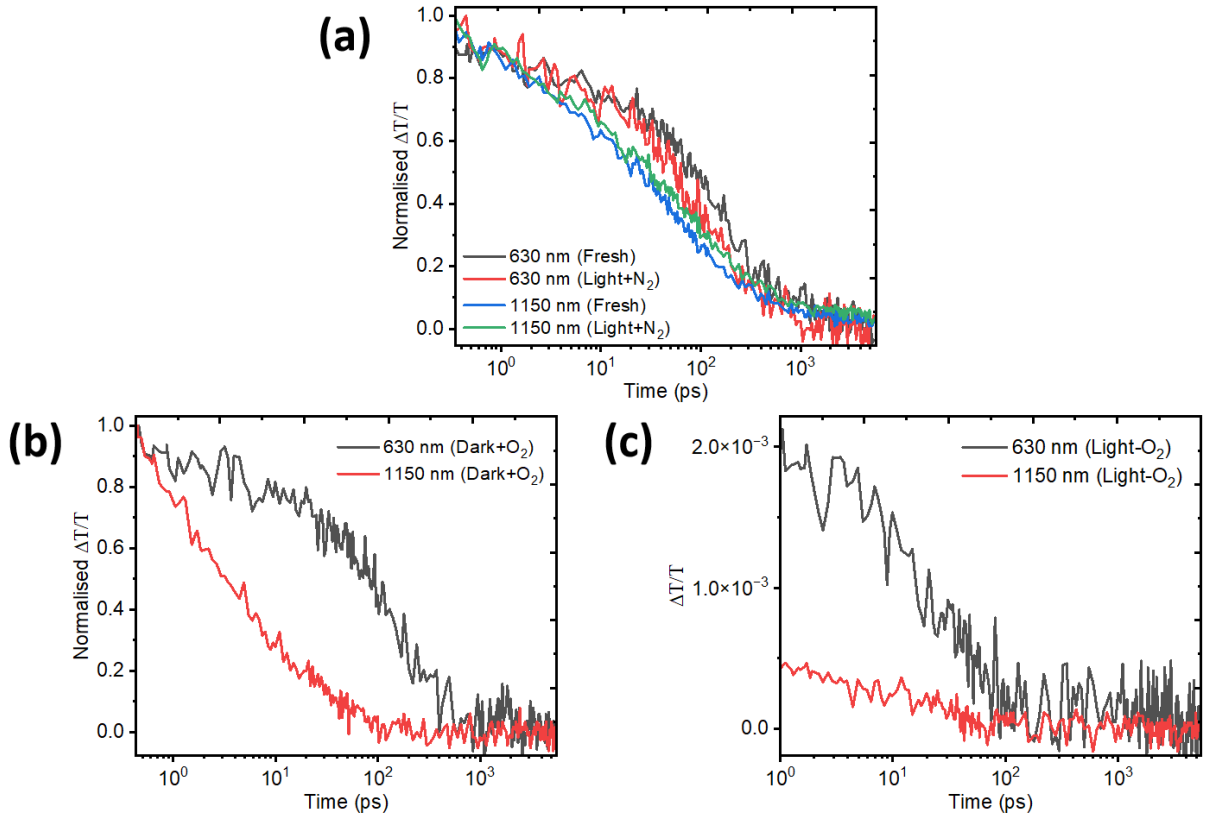

Figure 4.5. The normalised kinetics of (a) Fresh and Light-N_2 PM6 films; (b) Dark-O_2 PM6 film; and (c) raw kinetics of Light-O_2 PM6 film at 630 nm and 1150 nm, excited at 580 nm with the fluence of 7.13μJ/cm^2 under room temperature 298K.

The kinetics of the signals at 630 nm (GSB) and 1150 nm (S1) are mirrored in Fresh and Light-N_2 films and all of them decay to zero around 1000 ps (Figure 4.5(a)), indicating the degradation caused by the light-soaking is negligible. Then we turn to compare the fs-TAS spectrum between Fresh and Dark-O_2 films. Surprisingly, there is an apparent quenching in both GSB and S1 signals (Figure 4.4(b)). The intensity of the GSB peak decreases slightly, while the S1 peak is quenched to almost half intensity with the same fluence excitation at 0.2 ps under oxygen exposure in the dark environment. Figure 4.5(b) illustrates the difference between the kinetics at 630 nm (GSB) and 1150 (S1) of Dark-O_2 film. The GSB signals of Dark-O_2 film decay entirely after a few thousand picoseconds, but the S1 signal decays to zero around 100 ps, which represents a faster decay in the S1 region in the presence of oxygen. The decay in S1 indicates the quench of singlet excitons. Since the amplitude of the entire spectrum gradually decays, the exciton quenching is due to the combination instead of dissociation. This is consistent with the oxygen-induced trap states hypothesis in PL results, which leads to increased non-radiative recombination. These observations show that oxygen already caused the PM6 film to degrade. For the Light-O_2 film, the spectrum of fs-TAS is changed completely (Figure 4.4(d)). The shape of GSB peaks varies and the GSB intensity is two times lower than that of Fresh PM6 film with the same fluence at 0.2ps. This change can be related to the absorption loss in the UV-vis spectrum

as stated in Figure 4.1(c). Meanwhile, the SE band (700-750 nm) quenches, with a new feature at 780 nm, which will discuss later. As Figure 4.5(c) shows, the intensity of the S1 peak at 1150 nm is nearly one-fourth of the GSB peak at 1 ps. The S1 and GSB peaks decay around 100 ps. The PM6 fs-TAS kinetics under light and oxygen exposure is more complex; we will discuss more details later.

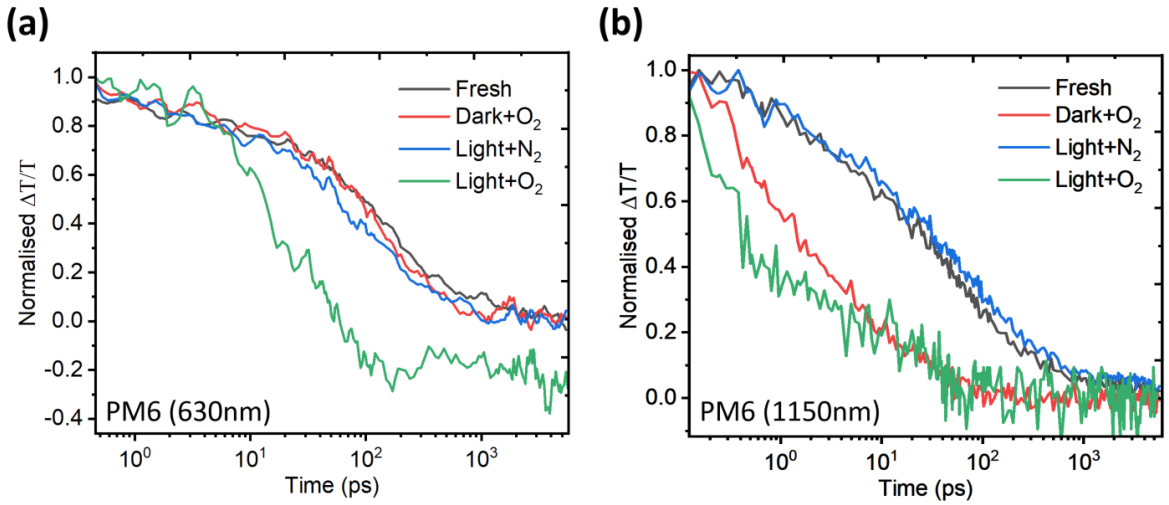

Figure 4.6. The normalised kinetics of ΔT/T results of the Fresh, Dark-O2, Light-N2, Light-O2 PM6 films (two-hour ageing time) at (a) 630nm GSB region and (b) 1150nm PIA region (S1), excited at 580 nm with the intensity of 7.13μJ/cm^2 under room temperature 298K.

The comparisons with the kinetics of fresh and aged films at 630 nm and 1150 nm are shown in Figure 4.6. At 630 nm, the decays of Fresh, Dark-O_2, and Light-N_2 are similar, which end at ~1000 ps under the same fluence. However, the GSB peak of Light-O_2 film has a faster decay towards zero at ~100 ps. The quench of PM6 GSB signals is consistent with the absorption loss under exposure to light and oxygen. In the S1 region, Fresh and Light-N_2 films have similar decay to zero at ~1000 ps, similar to their GSB signals. However, the S1 kinetics of the Dark-O_2 sample shows a faster decay under the same excitation fluence, which ends around ~100 ps, representing the singlet exciton quenching as discussed before. The decay in the S1 peak of Light-O_2 film is even faster than the one of Dark-O_2 condition, which means more excitons are quenched under the combined effect of light and oxygen exposure.

The fluence series of kinetics at GSB and S1 peaks are plotted in Figure 4.7 and Figure 4.8 to distinguish between the geminate (monomolecular) and non-geminate (bimolecular) recombination. Geminate recombination, referring to the recombination of an electron and hole by the quenching of a single exciton[88–90], can repopulate the ground state or a triplet exciton state[91,92]. In either case, there is a monomolecular loss mechanism, which lowers quantum efficiency by a fixed factor at all excitation intensities. Therefore, the fluence independence attributes the geminate recombination. Non-geminate recombination is the recombination of two free opposing charges. The density of the

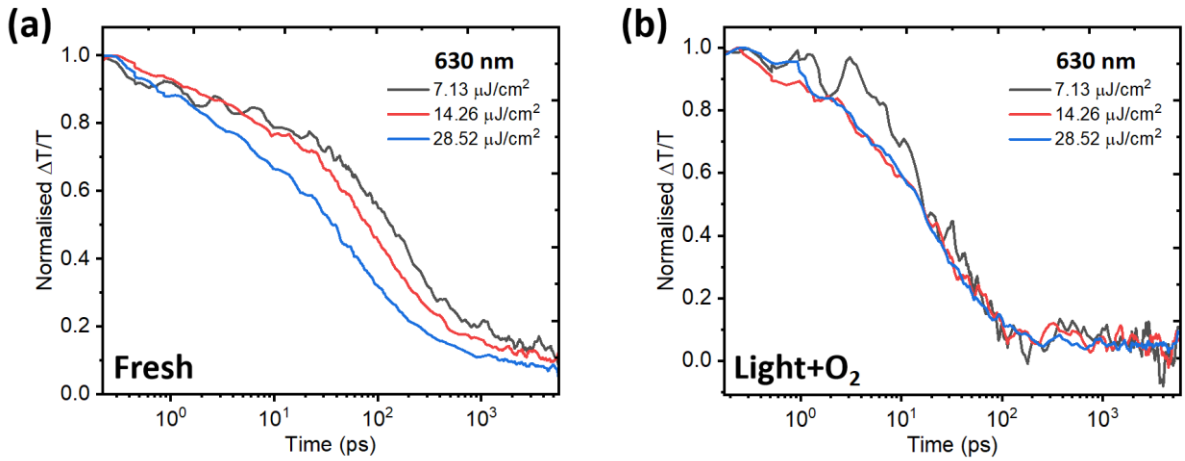

Figure 4.7. The normalised fluence series kinetics of the (a) Fresh PM6 film, and (b) Light-O_2 PM6 film at 630 nm after 580 nm excitation under room temperature 298K.

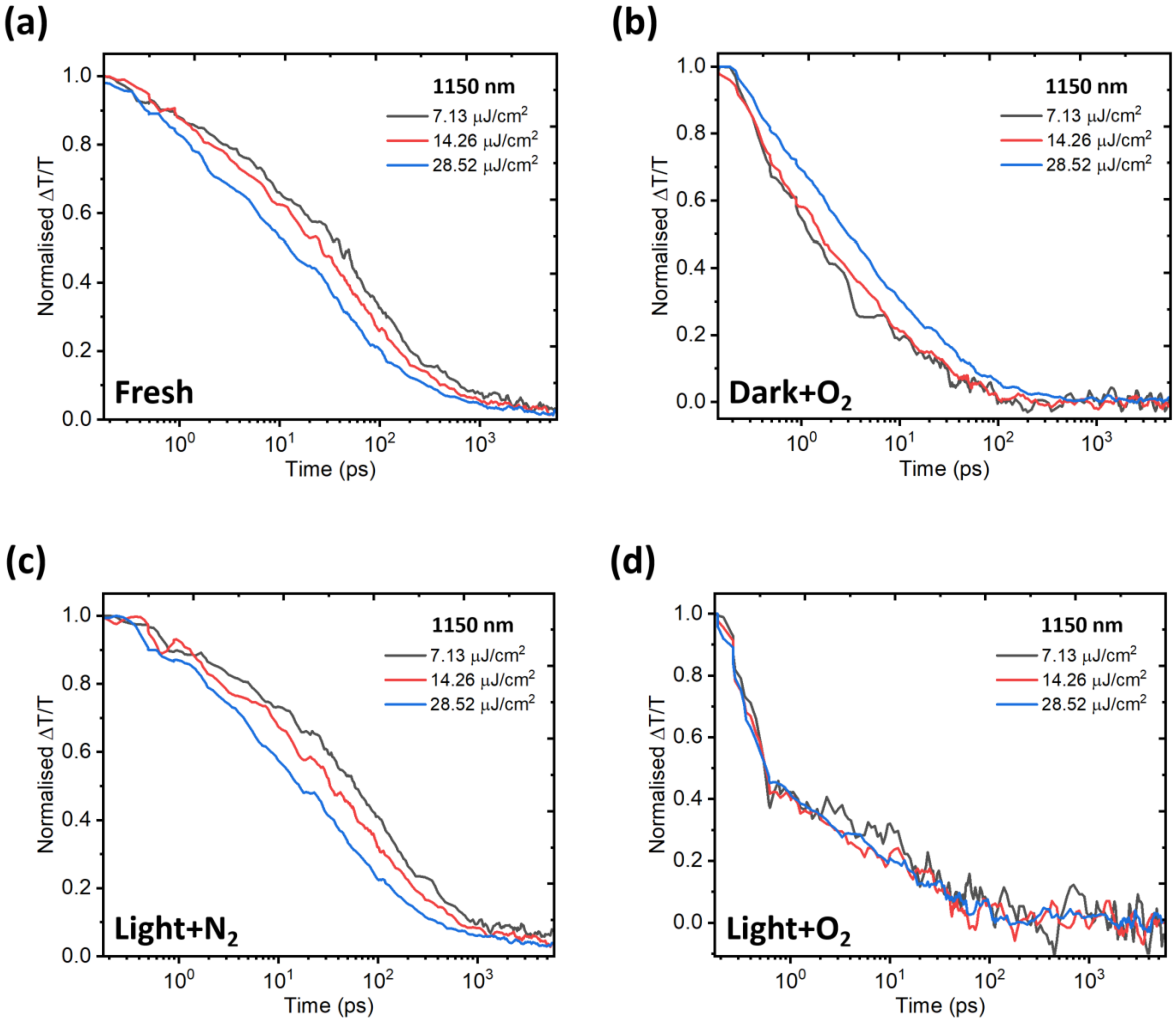

Figure 4.8. The normalised fluence series kinetics of the (a) Fresh PM6 film, (b) Dark-O_2, (c)Light-N_2, (d) Light-O_2 PM6 films (two-hour ageing time) at 1150 nm after 580 nm excitation under room temperature 298K.

spatially separated (or free) charges determine the rate of non-geminate recombination, which means that the strength of the light illumination affects this rate, so high fluence dependence reveals intensity-dependent non-geminate recombination[93]. The strong fluence dependence appears at the GSB (630 nm) peak in the Fresh PM6 film (Figure 4.7(a)). Higher fluences cause more rapid decay, which represents that there is bimolecular recombination. The Dark-O_2 and Light-N_2 films show the same fluence dependence as the Fresh PM6 film. In contrast, the fluence of Light-O_2 film at the GSB peak is closer to independence. The decays have the same kinetics with higher fluences, suggesting monomolecular recombination (Figure 4.7(b)), which raises the trap state. The fluence series of PM6 kinetics at the S1 peak (1150 nm) of four conditions are shown in Figure 4.8. Similar fluence dependence is observed in the S1 region in Fresh and Light-N_2 films. Faster decays resulted in higher fluences, revealing the non-geminate (bimolecular) recombination. In Dark-O_2 film, the decays of fluence 7.13μJ/cm^2 and 14.26 μJ/cm^2 have similar kinetics, but the S1 signal of the fluence 28.52 μJ/cm^2 decays slower, which means it is not a bimolecular recombination process. A clear fluence independence relationship is found in the Light-O_2 film. The decays remain the same under stronger fluence, indicating that monomolecular recombination is taking place, similar to the GSB decay. The monomolecular recombination in both GSB and S1 decays of the Light-O_2 PM6 film means trap states may be generated after exposure to oxygen and light.

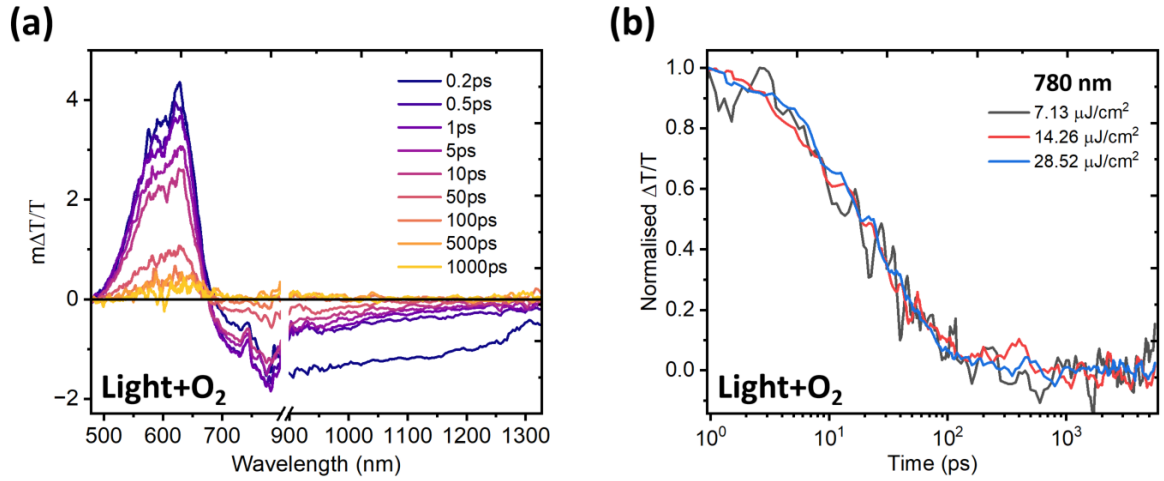

Figure 4.9. (a) The fs-TAS spectrum of Light-O_2 PM6 film; (b) The normalised fluence series kinetics of the Light-O_2 PM6 film with fluence 14.26 μJ/cm^2, after 580 nm excitation under room temperature 298K.

To investigate more details in Light-O_2 condition, the spectrum of Light-O_2 PM6 film with excitation fluence of 14.26 μJ/cm^2 at 580 nm is shown in Figure 4.9(a). Compared with the Fresh PM6 film (Figure 4.4), the SE signals have an apparent quenching in Light-O_2 condition, as well as the GSB signals, which allocates the depopulation of excitons. We can see that a new feature occurs in the negative ΔT/T region near 780 nm. According to these spectral evolutions, the intrachain excitons are more likely to relax into a non-emissive excited state than the ground state[94]. The non-emissive state is possible to be related to polarons. Free

polarons (separated polarons without Coulomb interaction) should have a longer lifetime than excitons because their recombination is constrained by slow polaron diffusion. The decay of the singlet exciton S1 peak is ~1000 ps (Figure 4.8(a)). However, the new species at 780 nm has a more rapid decay of ~100 ps (Figure 4.9(b)). This attributes that the non-emissive excited state is not PM6 polaron. As Figure 4.9(b) indicates, the fluence independence of kinetics at 780 nm contributes to the geminate recombination, which is possible to assign with polaron pairs[94] (also called spatially indirect excitons[95–97]). The polaron-pair recombination process avoids polaron diffusion. As a result, the recombination of polaron pairs can proceed much quicker than free polarons. The polaron pairs are bound states, which impedes the charge separation process. Therefore, non-radiative recombination increases, which explains the degradation in Light-O_2 PM6 film. In fs-TAS spectra, we found exciton quenching and faster decay at exciton S1 region under dark and oxygen conditions, suggesting the possible starting point of the PM6 degradation process is related to the oxygen exposure. A new-formed bound polaron-pair state and geminate recombination as well as a larger exciton quenching indicate that light exposure may accelerate the degradation and form new species in PM6, suggesting the possible chemical structure change in PM6.

4.1.3 Slow-TAS

To explore the photophysics of PM6 film under ageing conditions on the microsecond timescale, the slow-TAS (ms-TAS) is employed for measurements. In PL and fs-TAS results, we found that the PM6 film has already degraded under the Dark-O_2 condition. The slow-TAS system is used to determine where the two reported oxygen-induced degradation pathways: singlet oxygen generation and superoxide radical anion, can cause the degradation of PM6 film. The energy transfer from the triplet excited state via intersystem crossing to molecular oxygen can generate singlet oxygen, which is highly reactive [42,43]. In this case, the oxygen can quench the triplet signal in ms-TAS due to the formation of singlet oxygen. It has been found that under a nitrogen environment, the quenched triplet signals can recover to their original lifetime in nitrogen[43,98]. The decay of triplet signals is exponential and fluence dependent. The superoxide radical anion is formed by the excited electrons transferred from organic materials to oxygen molecules[99–101]. The trap-assisted bimolecular recombination of polarons reveals the formation of radical ions in organic materials[53]. In ms-TAS, the decay of a polaron signal can be fitted into a power law function[102,103]. The oxygen quenching of polaron signals represents the radical ions reacting with the molecular oxygen, generating superoxide radical anion. However, Figure 4.10 states that the Fresh PM6 film has no signal at 850 nm on the microsecond time scale. Once exposed to oxygen for two hours in the dark, a small and rapid signal is found at 850 nm. No oxygen quenching of signals attributes that the oxygen-induced degradation in PM6 film

is not associated with either singlet oxygen or superoxide radical anions. To better understand whether the signal at 850 nm comes from the physical interaction or the chemical reaction with the molecular oxygen and PM6 film, we place the PM6 film back in a nitrogen environment under the dark condition for 2 hours as well. If it is a physical interaction, when molecular oxygen is removed from the surface of PM6 film, the signal should recover to the original kinetics under a nitrogen condition. If not, it means that the oxygen has caused irreversible degradation in PM6, causing the chemical structure change in PM6. Clearly, the signal at 850 nm remains after the second exposure of nitrogen (Figure 4.10), suggesting a irreversible chemical reaction is more likely to occur between molecular oxygen and PM6.

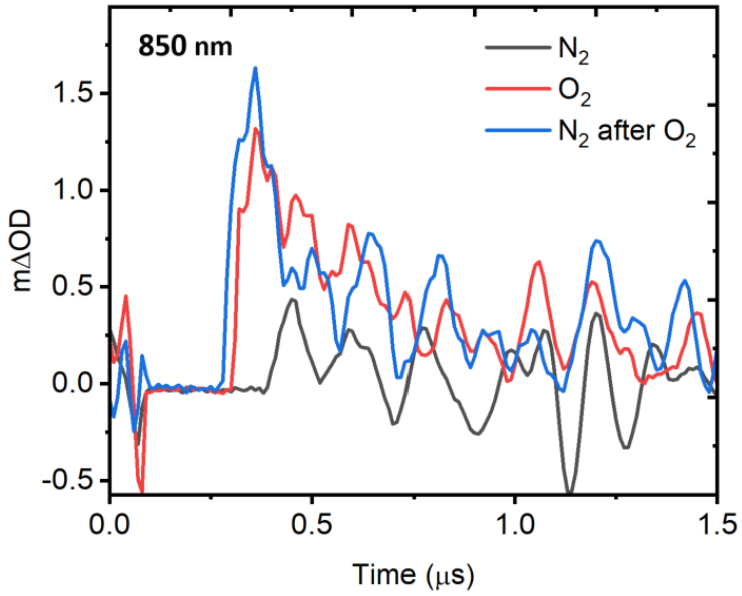

Figure 4.10. The transient absorption kinetics of PM6 film under nitrogen (2-hour), oxygen (2-hour) and nitrogen (2-hour) environment again, excited at 532 nm and probe at 850 nm with 458 μJ/cm^2 fluence.

The comparisons of PM6 ms-TAS spectra between the first and second nitrogen environments after oxygen exposure are shown in Figure 4.11. The negative peak at 650 nm assigns the GSB of PM6. The GSB peak under the N_2 and N_2-O_2-N_2 remains similar kinetics, which decays after 1 μs. This indicates no obvious change in absorption of PM6, which is consistent with UV-vis results. However, a positive species is shown around 800-950 nm after exposure to oxygen, and it remains under the second nitrogen exposure (Figure 4.11(b)), which has a rapid decay of ~0.5 μs. The new signal may relate to the $PM6^+$ species. As reported, oxygen may induce electron trap[104], which traps the dissociated electrons, leading to the accumulated holes. Compared with the results of the Dark-O_2 film, the ms-TAS spectrum and kinetics of the Light-O_2 film are slightly different. There is a signal at 850nm in the Light-O_2 PM6 film (Figure 4.12.(a)). However, a GSB peak shift at 600 nm is observed in the spectrum (Figure 4.12.(b)), which corresponds to the absorption peak change in the UV-vis spectrum (Figure 4.1.(c)). Meanwhile, the GSB peak decays faster

(~0.5 μs) in Light-O_2 film than Dark-O_2 film. The new peak at 850 nm is also found under the Light-O_2 condition, but it decays slower (~1 μs) than the one under the Dark-O_2 environment. It suggests that light exposure may accelerate the degradation and cause more severe degradation of PM6 chemical structure.

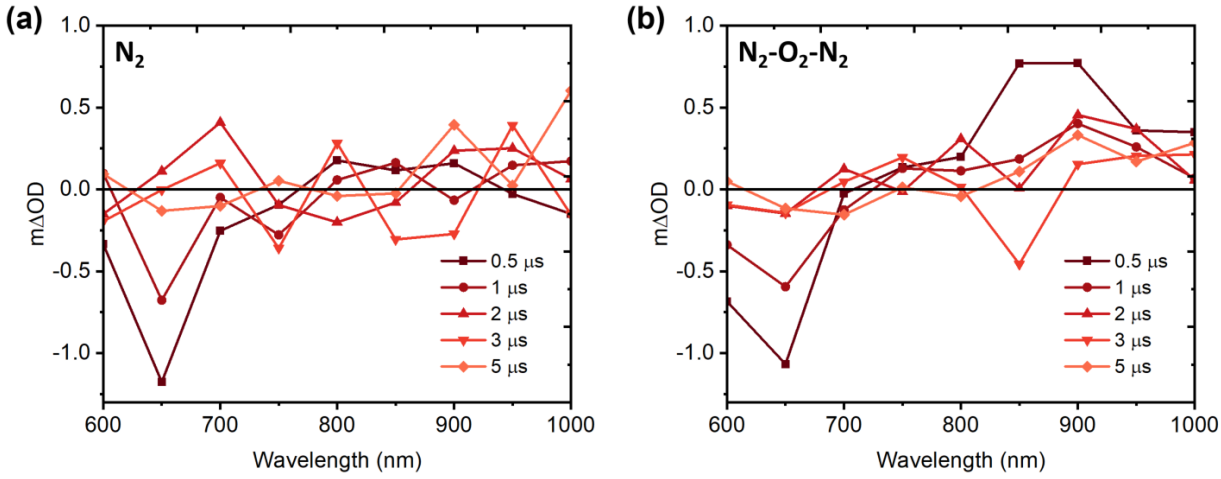

Figure 4.11. The transient absorption spectra of PM6 film under (a) nitrogen (2 hours) and (b) nitrogen environment (2 hours) after the oxygen exposure (2 hours) in the dark at different delays times, excited at 532 nm with 458 μJ/cm^2 fluence.

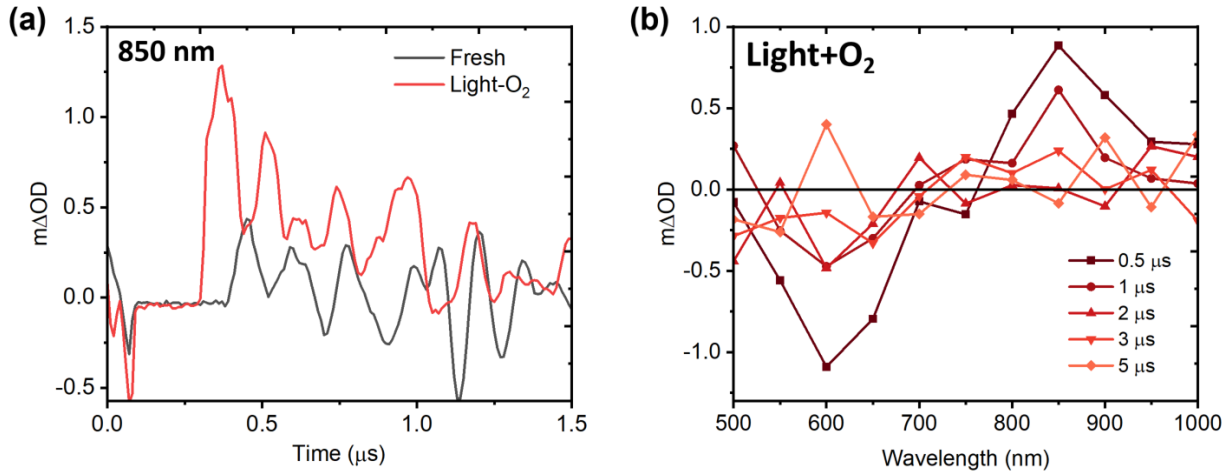

Figure 4.12. (a) The transient absorption kinetics of Fresh PM6 film and Light-O_2 PM6 film (2-hour ageing time) at probe wavelength 850 nm; (b) The spectrum of Light-O_2 film at different delays time, excited at 532 nm with 458 μJ/cm^2 fluence.

4.2 PTQ10

4.2.1 UV-vis Spectroscopy

UV-vis spectroscopy was employed to investigate the absorption spectra of PTQ10 films during the ageing process. For the Fresh PTQ10 film, the absorption spectrum contains two absorption bands from 300 nm to 700 nm, typical for D–A copolymers[78]. There is a weak absorption band at ~345 nm. The absorption peak is ~601 nm with a shoulder peak at ~557 nm. We compared the absorption spectra of fresh and aged PTQ10 films in Figure 4.13. In the Dark-O_2 condition, the absorption spectrum is almost no change. The absorption under Light-N_2 and Light-O_2 environments show a similar spectrum. Both situations resulted in a slight decrease of the absorption peak at ~601 nm, suggesting light-soaking leads to a weak absorption loss of PTQ10 films. In comparison, under combined light and oxygen exposure, PTQ10 shows good stability based on UV-vis absorption results, which is better than PM6.

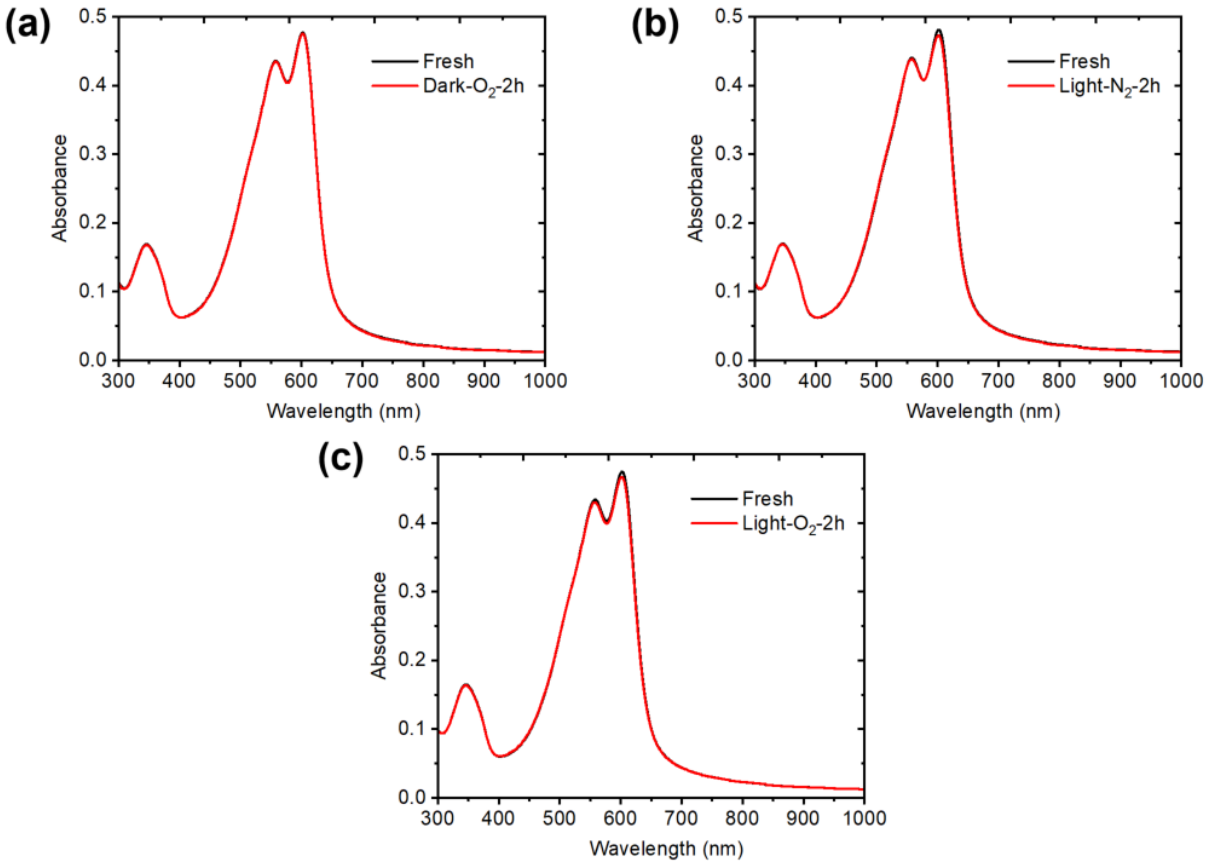

Figure 4.13. The UV-vis spectrum of Fresh, (a)Dark-O_2, (b)Light-N_2, (c)Light-O_2 PTQ10 films under the simulated sunlight (without UV light) and oxygen atmosphere for 2 hours.

4.2.2 PL Spectroscopy

As reported, UV-vis spectroscopy is less sensitive than PL spectroscopy, especially for organics materials [87]. To observe minor differences between fresh and aged PTQ10 films, PL spectroscopy is utilised to measure the photoluminescence emission. According to Figure 4.14, the peak at 720 nm in the PL spectrum is due to the band-to-band transition in the PTQ10 polymer. The Stokes shift, described in section 3.6, assigns the red shift between the absorption and emission spectra. Clearly, the Stokes shift in PTQ10 film is ~119 nm, larger than the one in PM6 film (~78 nm). Figure 4.15(a) states the PL spectrum difference of PTQ10 films under four conditions. The PL peak intensity has the relationship where Fresh > Dark-O_2 > Light-N_2 > Light-O_2. The quenching in the PL spectrum represents the increased non-radiative recombination. The light-N_2 film has a lower peak than the one of the Dark-O_2 film, indicating that light exposure can cause more non-radiative recombination than oxygen. A huge quenching rate was observed in the Light-O_2 condition, where the PL peak decreased 64% compared with Fresh PTQ10 film (Figure 4.15(b)). The significant quenching in the PL spectrum reveals that far more non-radiative recombination is generated under light and oxygen. In this case, combined exposure of light and oxygen has the biggest impact on the stability of neat PTQ10 film. Compared with the PL quenching of PM6 films (Figure 4.3), PTQ10 shows better photochemical stability in PL measurements.

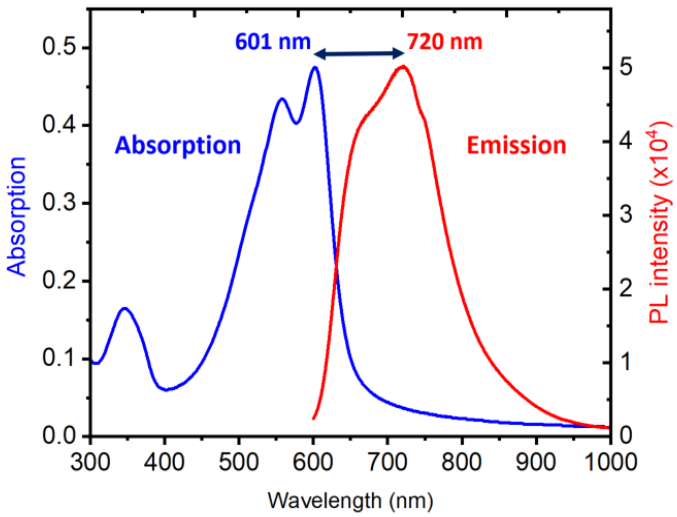

Figure 4.14. The Stokes shift between the UV-vis absorption and PL emission spectrums of fresh neat PTQ10 film, excited at 532 nm with intensity of 45 mW/cm^2.

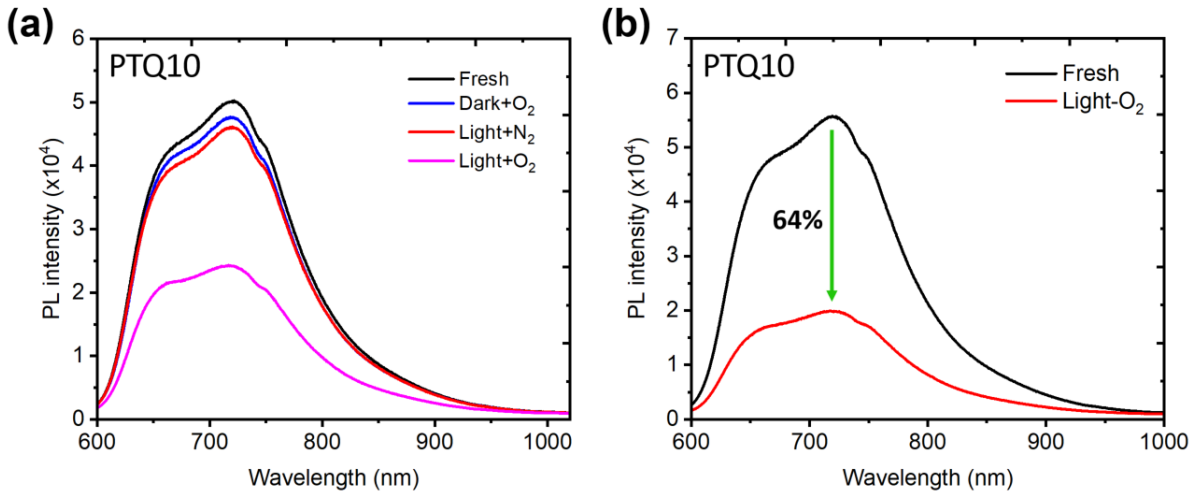

Figure 4.15. (a) The PL spectrum of Fresh, Dark-O_2, Light-N_2, Light-O_2 PTQ10 films (two-hour ageing time); (b) The quench of PL peak in Fresh and Light-O2 PTQ10 films, excited at 532 nm with the intensity of 45 mW/cm^2.

4.2.3 Fs-TAS

The femtosecond transient absorption spectroscopy was employed for PTQ10 films under different ageing conditions. The spectra of TAS kinetics in fresh and aged films are shown in Figure 4.16, excited at 580 nm with a low fluence of 7.13 μJ/cm^2. The signal from 500 nm to 650 nm assigns the GSB of PTQ10 film, and the maximum is at 611 nm. The SE signal is around 650-750 nm, which attributes the emission of excitons. In the NIR range, the peak at 1180 represents the PIA of PTQ10, which comes from the formation of singlet excitons S1. The variations of peak amplitude in Figure 4.16 are related to the film thickness, which is irrelevant to our topic. Therefore, we will focus on the discussion TAS spectrum and decay kinetics. There is no obvious spectrum change in comparisons between fresh and aged PTQ10 films.

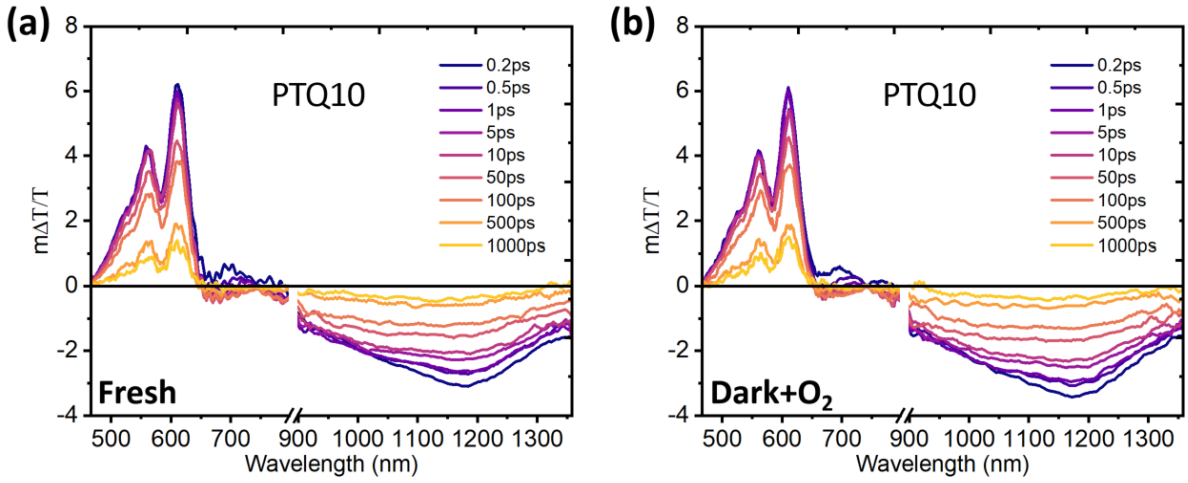

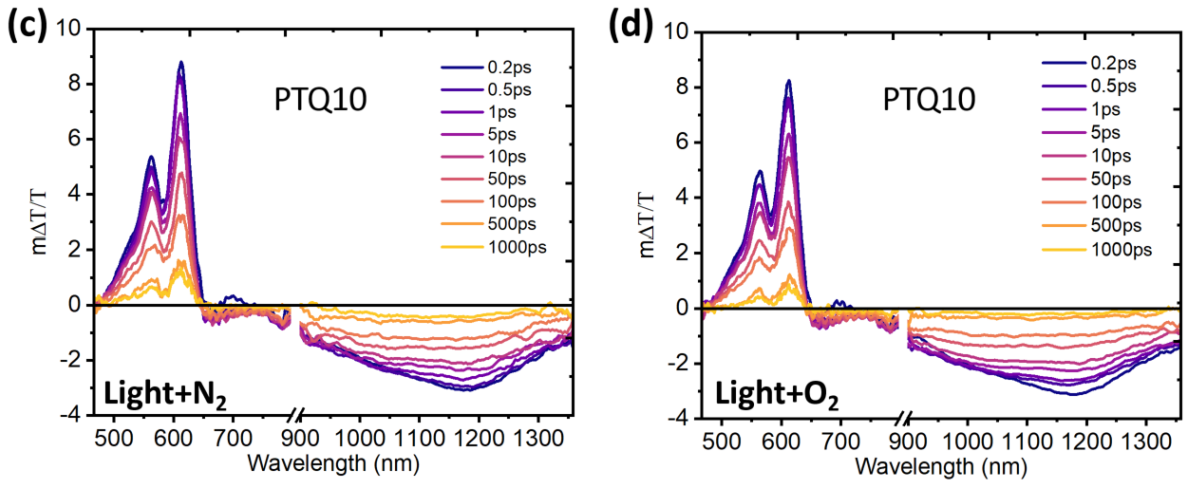

Figure 4.16. The fs-TAS spectra of the (a) Fresh, (b) Dark-O2, (c) Light-N2, (d) Light-O2 PTQ10 films (two-hour ageing time), excited at 580 nm with the intensity of 7.13 μJ/cm^2 under room temperature 298K.

Then, we turn to compare the decay kinetics. In Figure 4.17 (a), the decay kinetics of GSB in Fresh and Dark-O_2 PTQ10 films are similar. However, the GSB peaks in Light-N_2 and Light-O_2 films show a faster decay, which indicates that light-soaking can accelerate the GSB in PTQ10 films. The decay kinetics of S1 peak is similar in Fresh, Dark-O_2 and Light-N_2 films. Only Light-O_2 film shows a slightly faster decay after 100 ps (Figure 4.17 (b)). Overall, compared with the GSB kinetics change, the decay of singlet exciton (S1) is almost the same under different conditions, revealing the that ageing process doesn't influence the exciton lifetime in PTQ10 films.

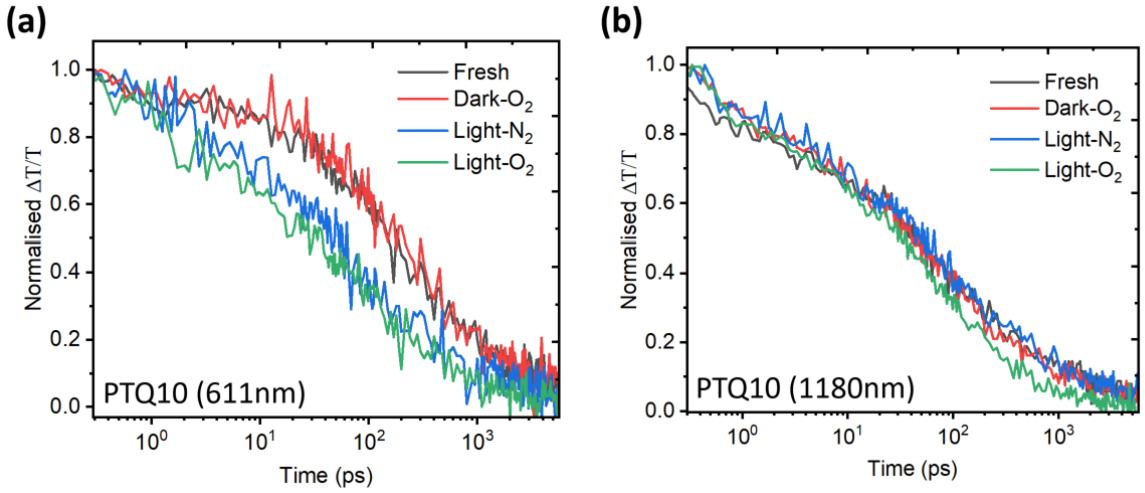

Figure 4.17. The normalised kinetics of ΔT/T results of the Fresh, Dark-O2, Light-N2, Light-O2 PM6 films (two-hour ageing time) at (a) 611nm GSB region and (b) 1180nm PIA region (S1), excited at 580 nm with the intensity of 7.13μJ/cm^2 under room temperature 298K.

Fluence dependent fs-TAS is utilised to distinguish the geminate (monomolecular) and non-geminate (bimolecular) recombination in PTQ10. As Figure 4.18 states, the decay of PTQ10 GSB signal is all fluence dependent under four conditions, where higher fluence leads to faster decay kinetics. Similarly, the S1 decays of PTQ10 films under four conditions are fluence dependent as well (Figure 4.19). The fluence dependent decay represents the bimolecular recombination, which means the trap state is unlikely to form in PTQ10 films. Therefore, PTQ10 films show excellent photochemical stability under exposure to light and oxygen. Note that there is no signal found in slow-TAS measurements, indicating that PTQ10 films have no long-lived state generation during the ageing process. In summary, the light exposure causes faster GSB decay in PTQ10, which implies that light may cause small degradation. Overall, PTQ10 is more stable under light and oxygen exposure than PM6.

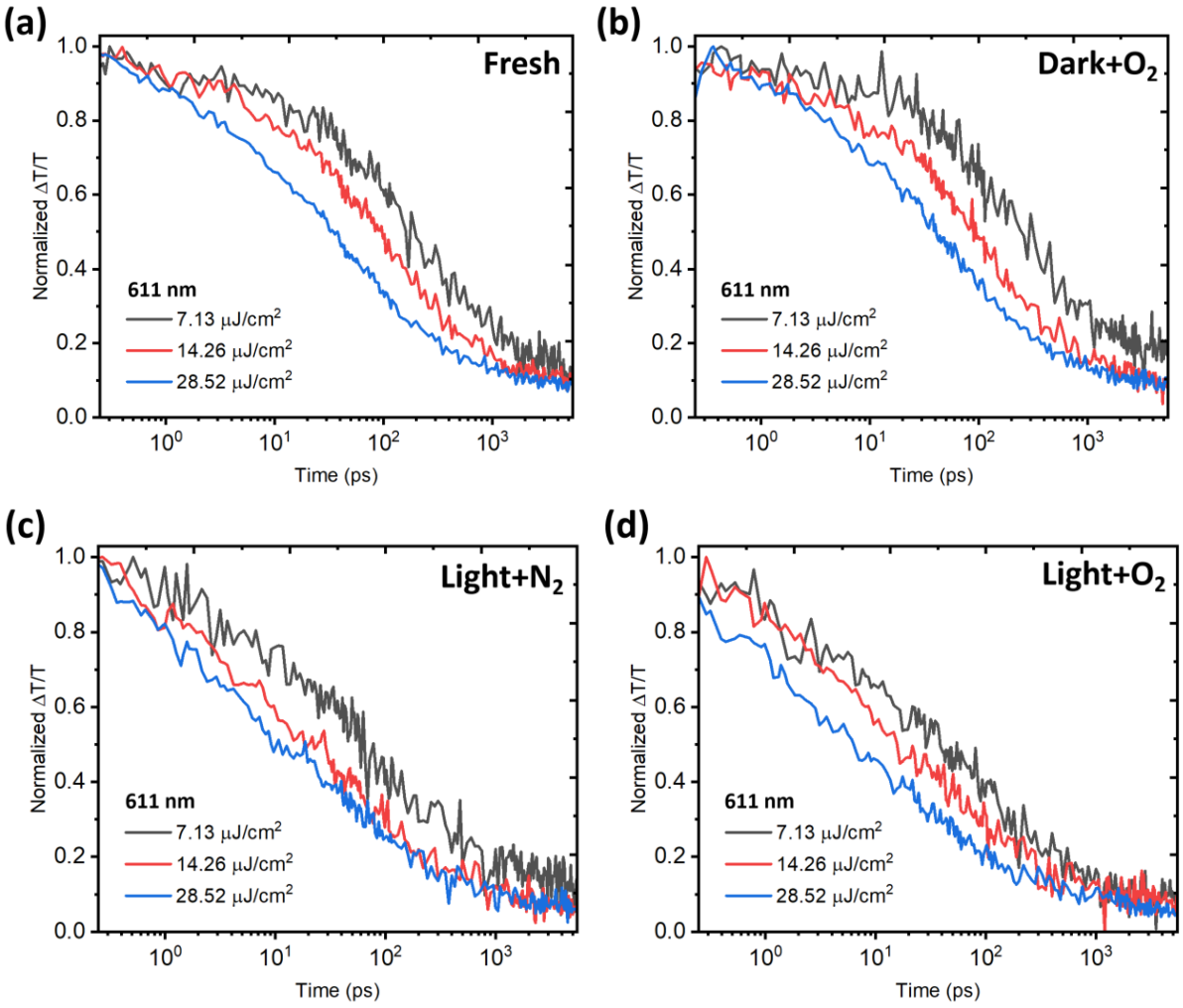

Figure 4.18. The normalised fluence series kinetics of the (a) Fresh PM6 film, (b) Dark-O_2, (c)Light-N_2, (d) Light-O_2 PTQ10 films (two-hour ageing time) at 611 nm (GSB) after 580 nm excitation under room temperature 298K.

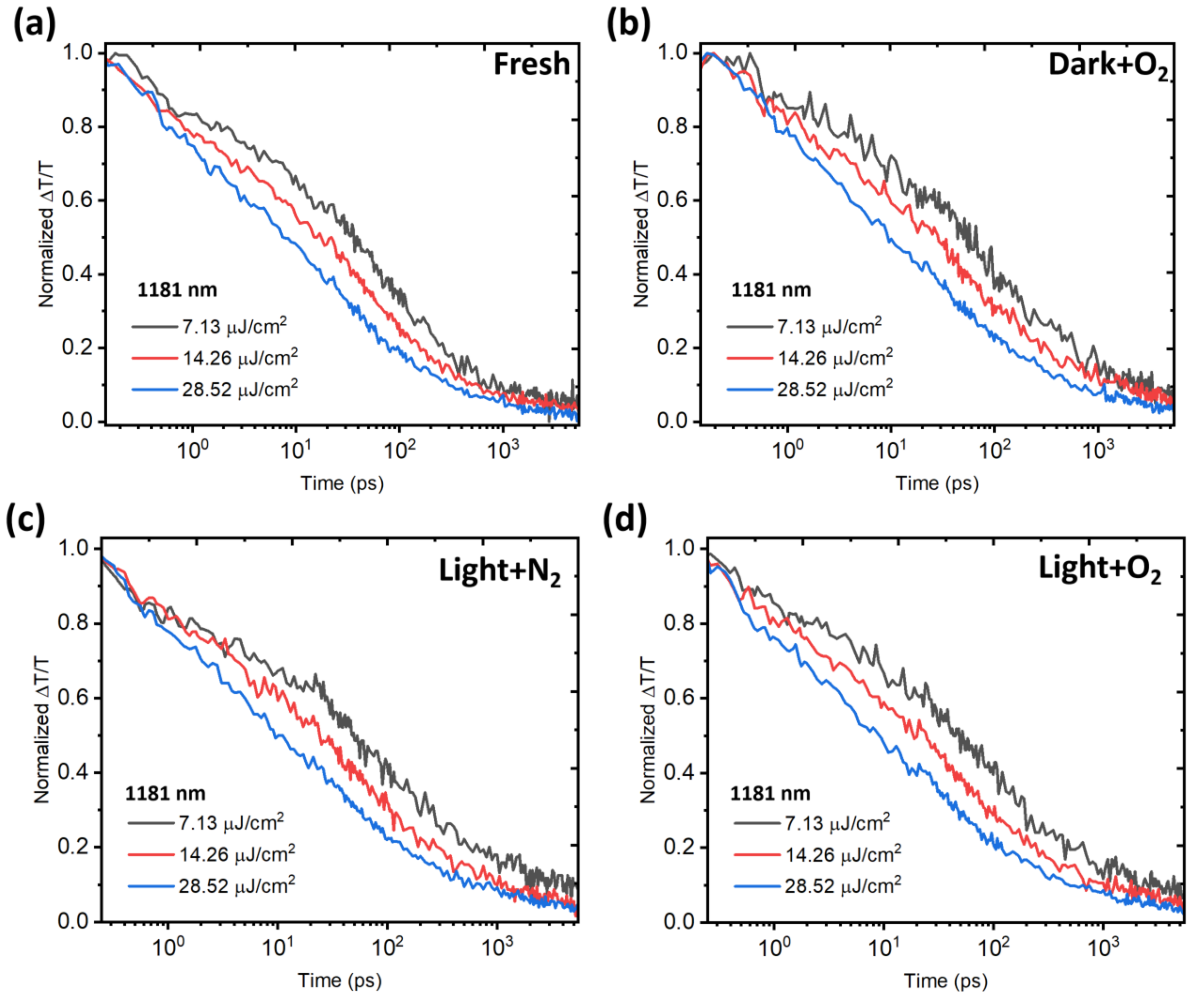

Figure 4.19. The normalised fluence series kinetics of the (a) Fresh PM6 film, (b) Dark-O_2, (c)Light-N_2, (d) Light-O_2 PTQ10 films (two-hour ageing time) at 1181 nm after 580 nm excitation under room temperature 298K.

Chapter 5. Discussion

5.1 Stability Differences between PM6 and PTQ10

Based on our results, PTQ10 shows a better photochemical stability than PM6 under same conditions of light and oxygen exposure. Both PTQ10 and PM6 are wide bandgap donor materials based on D-A copolymerization (Figure 3.1). There are two hypotheses related to the stability difference between PTQ10 and PM6 neat films.

5.1.1 Crystallinity

A difference between GIWAXS measurements of neat PTQ10 film and PM6 film has been reported (Figure 5.1)[105]. The π–π stacking diffraction peaks ((010) peak) are found in both PTQ10 and PM6 films in the out-of-plane (OOP) direction, indicating that face-on molecular orientation. The PTQ10 and PM6 films have π–π stacking diffraction peaks at 1.77 and 1.72 $Å^{-1}$, which equals the π–π stacking distance of 3.55 and 3.66 $Å^{-1}$ (Table 1). The π–π stacking coherence length (CL) is calculated from the Scherrer equation $CL = \frac{2\pi K}{\Delta q}$, where Δq is the peak width and K is the shape factor[106]. For PTQ10 and PM6 films, π–π stacking CLs in the OOP direction are 28 and 20 Å, respectively. This result demonstrates that PTQ10 processes a higher level of molecular crystallinity in the face-on orientation. In comparison, PTQ10 film has a smaller π–π stacking distance than PM6 film, which should be associated with the simpler chemical structure of PTQ10.

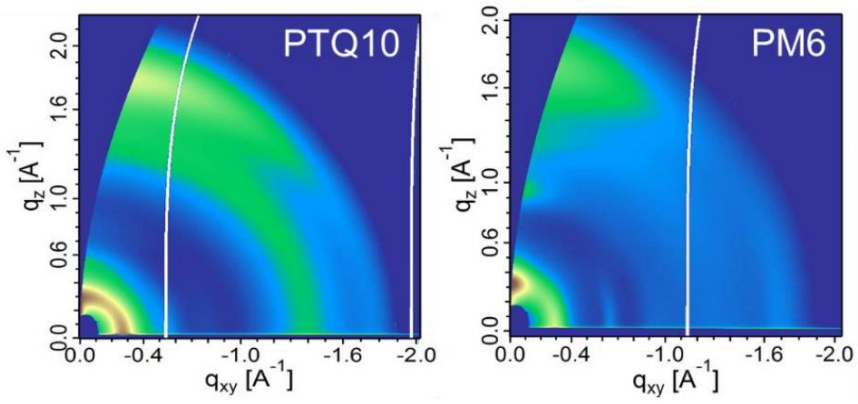

Figure 5.1. The 2D GIWAXS patterns of the neat PTQ10 and PM6 polymer films[105].

Sample	q [010] [Å^{-1}]	d [010] [Å]	Δq [010] [Å^{-1}]	CL [010] [Å]
PTQ10	1.77	3.55	0.222	28
PM6	1.72	3.66	0.321	20

Table 1. The GIWAX data of PTQ10 and PM6 neat films, where q is the scattering vector, d is the $\pi - \pi$ stacking distance, Δq is the peak width, CL is the coherence length[105].

These observations imply a tighter and more ordered molecular face-on packing contained in PTQ10 film rather than PM6 film, which is beneficial for charge transport[105]. Therefore, the film morphology is easier to change in PM6 during ageing treatment, inducing defects which contribute to the trap states. The trap states can influence the properties of PM6 as section 4.1 explained. This may be one reason for the stability difference between PTQ10 and PM6 films.

5.1.2 Molecular Structure

It has been reported that donor groups show different photochemical stability[107]. As Figure 5.2 states, PM6 is a benzo [1,2-b:4,5-b'] dithiophene (BDT)-based polymer donor and PTQ10 is a thiophene-based polymer donor[108]. The BDT donor unit has been reported for its instability under light and oxygen exposure. In excited states, the BDT group reacts with oxygen rapidly, contributing to the irreversible main-chain conjugation disorder and reduced hole mobility[109]. This observation supports our observations that oxygen exposure may cause irreversible chemical structure change in PM6, which can be proved by Raman Spectroscopy and nuclear magnetic resonance spectroscopy (NMR) in future work. In contrast, the thiophene donor group showed very good stability, which degraded fully after > 600 hours of illumination under an ambient environment[107]. The degradation stage of the thiophene ring was detected after 200 hours of irradiation via IR spectroscopy. This supports our finding that PTQ10 film has good photochemical stability but still needs more measurements to prove it. Therefore, different chemical structures are associated with the photochemical stability difference between PM6 and PTQ10.

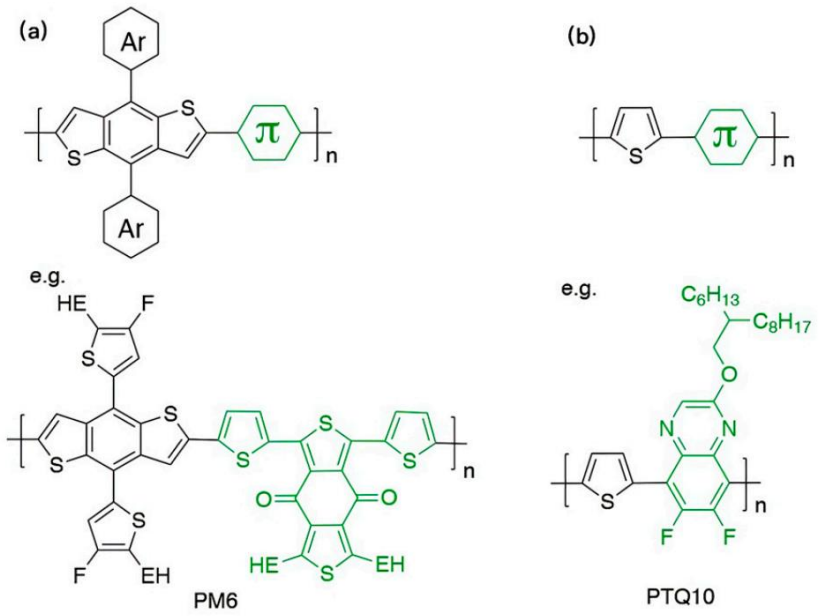

Figure 5.2. Chemical structure of (a) PM6 (BDT-based), (b) PTQ10 (thiophene-based)[108].

5.2 Comparisons with Other Donors

To better understand the how stable PTQ10 and PM6 are, four wide-used donor materials PBDB-T, D18, P3HT and PTB-7 are selected for photochemical stability comparisons.

5.2.1 PBDB-T and D18

PBDB-T(Poly[(2,6-(4,8-bis(5-(2-ethylhexyl)thiophen-2-yl)-benzo[1,2-b:4,5-b']dithiophene))-alt-(5,5-(1',3'-di-2-thienyl-5',7'-bis(2-ethylhexyl)benzo[1',2'-c:4',5' c']dithiophene-4,8-dione)]) and D18 (Poly[(2,6-(4,8-bis(5-(2-ethylhexyl-3-fluoro)thiophen-2-yl)-benzo[1,2-b:4,5-b']dithiophene))-alt-5,5'-(5,8-bis(4-(2-butyloctyl)thiophen-2-yl)dithieno[3',2':3,4;2'',3'':5,6]benzo[1,2-c][1,2,5]thiadiazole)]) are both wide bandgap polymer donor materials, which pairs well with narrow bandgap NFAs (Figure 5.3). When PBDB-T is blended with the new polymer acceptor PN-Se, a high PCE of 16.16% is achieved[110]. The device of D18:2BTH-2F blend reached the highest PCE 15.44% among unfused-ring small molecule acceptor blends[111]. Since PBDB-T and D18 systems also have good device performances, they are chosen to compare the photochemical stability with PM6 and PTQ10. Under the same AM1.5G illumination in the ambient atmosphere overnight, the absorption loss of four donor films is indicated in Figure 5.4 respectively. PBDB-T and D18 show similar degradations but are slightly larger than PM6 in absorption spectra when films are aged overnight. On the other hand, there is almost no change in

PTQ10 absorption even under ageing conditions overnight. Based on the UV-vis absorption spectra change, the photochemical stability of polymer donor materials has a relationship that PTQ10 >> PM6 > PBDB-T/D18. This finding still needs more experimental evidence, but it gives us an idea that PM6 has relatively better photochemical stability than PBDB-T and D18. Meanwhile, PTQ10 is more stable than other commonly used donor materials.

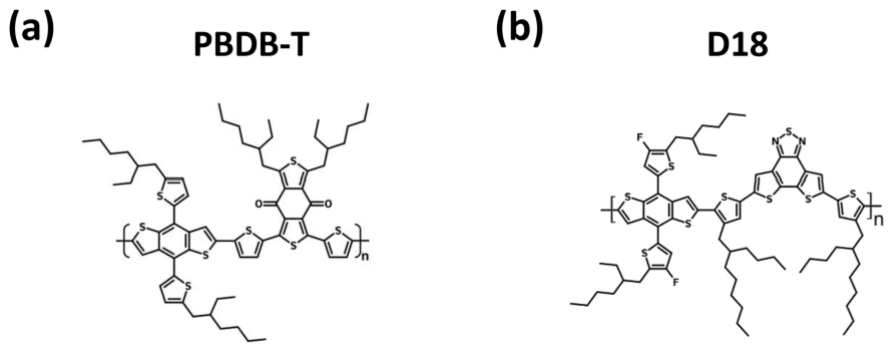

Figure 5.3. Chemical structure of (a) PBDB-T and (b) D18 donor materials.

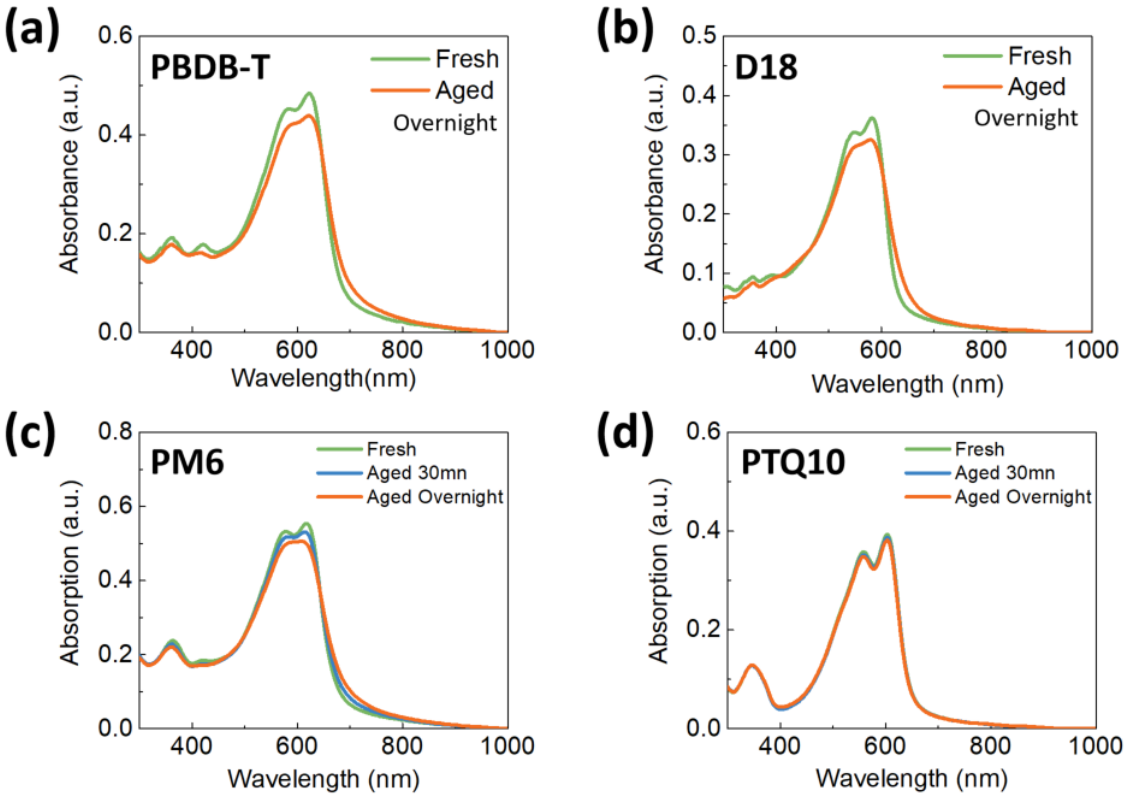

Figure 5.4. The UV-vis absorption degradation of neat (a) PBDB-T film, (b) D18 film, (c) PM6 film and (d) PTQ10 film under AM1.5G irradiation (without UV light) under ambient environment. (Adopted from unpublished work of Dr Yiwen Wang)

5.2.2 P3HT

Poly(3-hexylthiophene-2,5-diyl) (P3HT) was first synthesised for fullerene acceptors (Figure 5.5(a)), but it also matched NFAs, in which a PCE of 9.46% is achieved based on the P3HT:ZY-4Cl device[112]. As reported, P3HT experiences severe photooxidation degradation[113]. The change in the P3HT UV-vis absorption spectrum records the irreversible degradation by illumination under an oxygen atmosphere (Figure 5.5(b)). The degradation rate is approximate to $dE/dt \approx 1\times10^{-5}\ s^{-1}$, where E is the absorbance peak at 554 nm (Figure 5.5(c)). For 2-hour degradation under combined exposure to light and oxygen, the absorption decreased roughly 11%. The degradation of P3HT is caused by the chain radical oxidation process, related to the oxidation ability of carbon atoms in the α position at the thiophene ring[114,115]. In our results, the absorption of PM6 decreased ~9.5% and PTQ10 had no relative change in the absorption spectra (Figure 4.1 and Figure 4.13). Therefore, we can conclude the photochemical stability comparison of these three donor polymers based on UV-vis absorption data, which PTQ1O >> PM6 > P3HT.

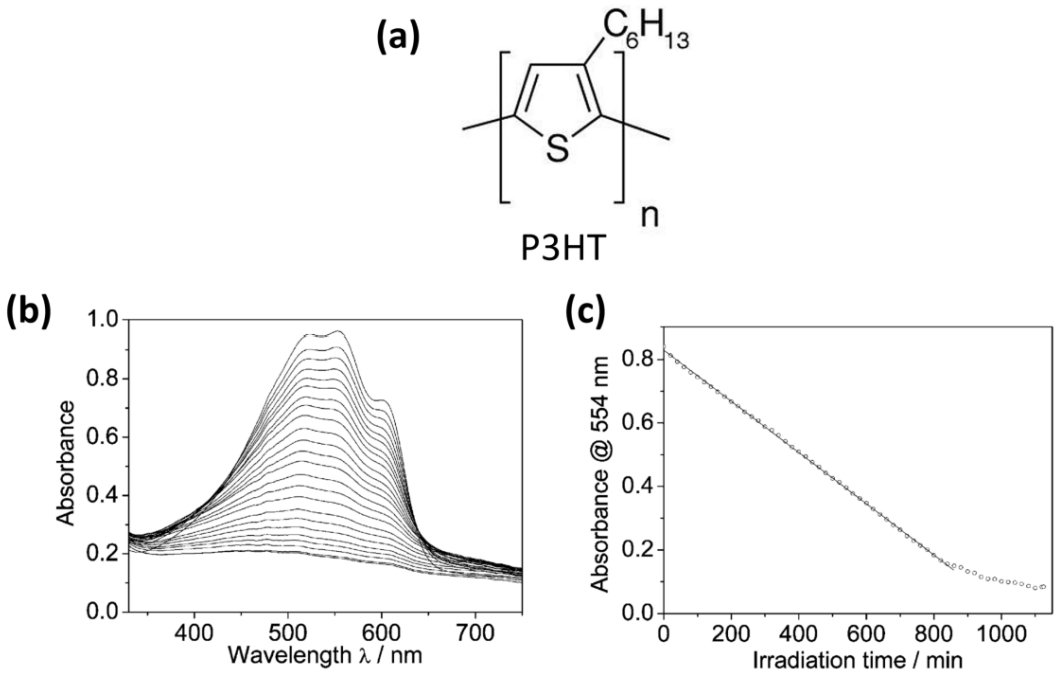

Figure 5.5. (a) Chemical structure of P3HT. (b) UV-vis absorption spectra of P3HT film with white LED light (~1 sun) and oxygen atmosphere. (c) The absorption degradation rate at 554 nm with irradiation time[116].

5.2.3 PTB7

The thieno[3,4-b]thiophene-alt-benzodithiophene (PTB7) based on the D-A copolymerisation (Figure 5.6(a))., which achieved 9.2% PCE with optimised PTB7:$PC_{70}BM$ devices[117]. A rapid photooxidation degradation has been observed in PTB7 neat films [118]. As Figure 5.6(b) demonstrates, after 4 hours of illumination in an oxygen atmosphere, the absorption maximum decreased ~60% in the PTB7 neat film, accompanied by a spectrum change. These results illustrate the super instability of PTB7 with combined exposure of irradiation and oxygen exposure. The instability of PTB7 comes from the formation of hydroxyl groups on the BDT unit after photooxidation [118], which supports our hypothesis that the BDT unit may cause degradation in PM6. Although PM6 has shown poor photochemical stability in our experiments, the absorption loss in the nest PM6 film is only ~9.5% after a 2-hour ageing process, which is much smaller than PTB7 films. Hence, PM6 has better photochemical stability than PTB7. PTQ10 neat films show no apparent degradation in the absorption spectrum under 2-hour combined exposure to light and oxygen, which reveals that PTQ10 has excellent photochemical stability. In summary, the photochemical stability of PTB7, PM6, PTQ10 follows the relationship, where PTQ10 >> PM6 >> PTB7. After a series of stability comparisons, we know that PM6 is relatively more stable than some other polymer donors, but PM6 still experiences severe degradation in the photooxidation process. However, PTQ10 has much better photochemical stability than most of the commonly used donors, including PM6.

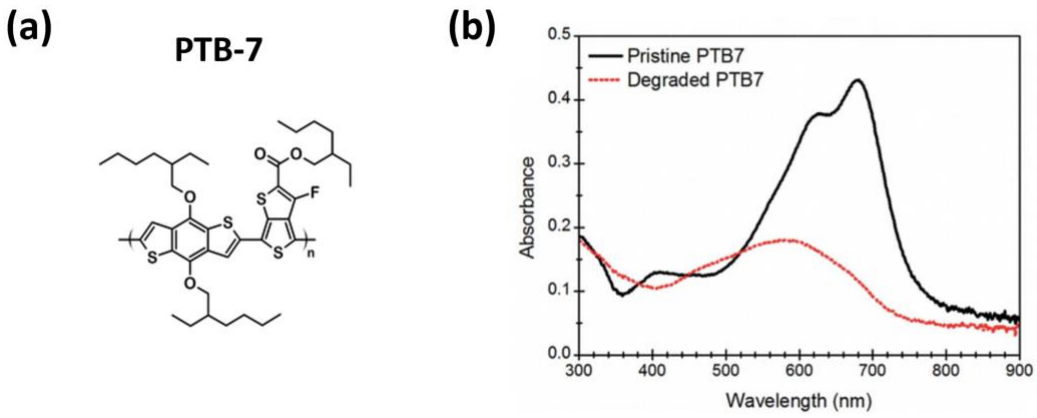

Figure 5.6. (a) Chemical structure of PTB7. (b) The absorption loss of a neat PTB7 film in UV-vis absorption spectrum under 4-hour white LED light (~1 sun) and oxygen exposure[118].

5.3 Applications

Since PM6-based and PTQ10-based OPV devices have significant PCEs ~20%, our observations about photochemical stability of PM6 and PTQ10 can apply to some commercial application aspects.

PM6

Based on our results, PM6 shows rapid degradation with oxygen exposure and better stability under only light exposure, which implies that PM6 is more reactive with oxygen than light. In which case, we should notice that PM6 is not suitable to spin coat in the oxygen atmosphere. Instead, it is better to prepare PM6 solution and spin coat films in the glovebox, which should lead to better device performance. The other thing is that the PM6 samples need to avoid oxygen during characterization measurements, otherwise the degradation may happen during experiments, which will affect the accuracy of the results. Considering the application area, PM6 is not a good choice for indoor and outdoor solar cells based on its oxygen-induced instability, which is a barrier to large-scale production. However, the aerospace application may consider the PM6 due to its better stability under light exposure.

PTQ10

We find that PTQ10 has great stability under light and oxygen exposure, and it is more environmentally stable than other widely used donor materials, such as PM6, P3HT and PTB7. The high stability gives PTQ10 more potential on application areas. PTQ10 already has advantages on cost and synthesis complexity. The price of PTQ10 per gram is estimated at 30.29 $, in contrast, the price of PM6 is 184.2 $ and PTB7 is 160.94$[119]. The synthetic route of PTQ10 is very simple, with only two-step reactions (Figure 5.7). On the other side, PM6 has a total of 11 synthetic steps and PBDB-T has 10 steps[120]. These advantages are important for commercialisation. In fact, although the development of donor materials is fast now, P3HT is still the dominant donor polymer for large-scale fabrications, because it is easy to synthesize and low cost[121]. However, as we stated in section 5.2.2, the efficiency of P3HT-based devices is not high (9.46%) [112]. Now, PTQ10 with high efficiency and stability can be a good candidate to replace P3HT in large area OPV fabrications. Meanwhile, it has been reported that PTQ10 has better stretchability than other donor polymers (eg. PM6, PTVT-T, PTzBI-Si)[122], which makes PTQ10 more promising for large-scale printing techniques like roll-to-roll systems. Due to the good photochemical stability, PTQ10 is appropriate for both indoor and outdoor applications and it has great potential for commercialisation.

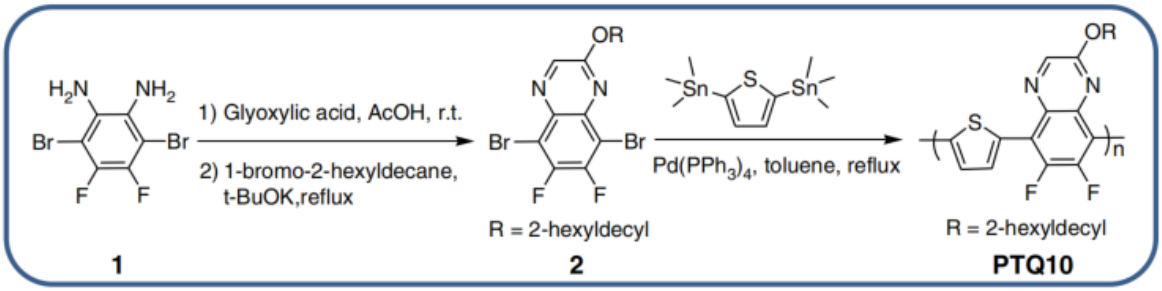

Figure 5.7. The synthesis steps of PTQ10[77].

Chapter 6. Conclusion and Future Work

6.1 Conclusion

In this project, we compared the photochemical stability of neat PM6 and PTQ10 films via different spectroscopic analyses. All results show that PTQ10 has better photochemical stability than PM6. To understand the origin of degradations in the PM6 neat film, three ageing conditions (Dark-O_2, Light-N_2, Light-O_2) of PM6 films are chosen for comparison. Through UV-vis spectroscopy, an apparent loss in vibronic peaks of the PM6 Light-O_2 film suggests possible increased energy disorder in PM6 domains. A larger PL peak quenching is observed in the Dark-O_2 film rather than the Light-N_2 film, as well as the PL spectrum of the Light-O_2 film disappeared. These results reveal the possible degradation pathway of PM6 is the oxygen-induced chemical reaction. Light exposure is likely to accelerate this degradation pathway and cause more severe degradation of PM6 chemical structure, which is further proved by TAS results. In fs-TAS measurements, there is no apparent difference between the Fresh and Light-N_2 PM6 films. In contrast, fluence-independent and faster decays are found in both Dark-O_2 and Light-O_2 films, which rationalises trap states in the monomolecular recombination. In addition, the formation of a new polaron-pair state appears in the Light-O_2 film, which may lower the charge generation rate. Slow-TAS results proved that the oxygen-induced degradation in PM6 is not associated with the singlet oxygen generation and superoxide radical anion. Instead, the oxygen exposure causes an irreversible change in PM6 and a long-lived signal (~1 μs) is generated in both Dark-O_2 and Light-O_2 PM6 films. In summary, the possible origin of degradations in PM6 is oxygen-induced chemical reactions and light exposure may accelerate this degradation pathway, causing the chemical structure change in PM6. The stability difference may be due to the crystallinity and molecular structure differences between PM6 and PTQ10. In summary, PTQ10 shows the best photochemical stability among PM6, PBDB-T, D18, P3HT and PTB-7 donor materials.

6.2 Evaluations and Future work

Since all measurements in this project are spectroscopy techniques, laser light exposure cannot be avoided during experiments. Therefore, samples in the Dark-O2 condition may still experience the light exposure by laser. Although we use low fluence excitation and take average data of repeated measurements, the effect of laser light still needs to be considered. Therefore, nuclear magnetic resonance may be a good tool to examine the chemical structure change of PM6 films under oxygen exposure without light influence in

the future, which analyses the molecular structure by interactions of nuclear spins. To determine whether the energy disorder increased in aged PM6 films, photothermal defection spectroscopy should be employed as well. Although the Slow-TAS results show oxygen exposure can cause an irreversible change to PM6 film, it still needs more experimental evidence. As we exposed the PM6 film under a nitrogen environment for only 2 hours after the oxygen condition, there is still a possibility that a few molecular oxygen remains on the PM6 surface, which causes interactions. Therefore, we will repeat fs-TAS experiments with a second nitrogen environment after the oxygen exposure for a longer time scale to double-check whether the oxygen-induced change in PM6 is irreversible or not. Since we proved the difference between photochemical stability of neat PM6 and PTQ10 films, it is worth comparing the device performances based on these two donor materials under the same conditions (Fresh, Dark-O_2, Light-N_2, Light-O_2) to see if the donor stability is associated with the device stability.

Reference

1. Tai, Q. & Yan, F. Emerging Semitransparent Solar Cells: Materials and Device Design. *Advanced Materials* vol. 29 Preprint at https://doi.org/10.1002/adma.201700192 (2017).

2. Chen, H. Y. *et al.* Polymer solar cells with enhanced open-circuit voltage and efficiency. *Nat Photonics* **3**, 649–653 (2009).

3. Research Cell Efficiency Records. *http://w w w.nrel.gov/ncpv/ images/efficiency _ chart.jpg* (2021).

4. Spanggaard, H. & Krebs, F. C. A brief history of the development of organic and polymeric photovoltaics. *Solar Energy Materials and Solar Cells* **83**, 125–146 (2004).

5. Benanti, T. L. & Venkataraman, D. Organic Solar Cells: An Overview Focusing on Active Layer Morphology. *Photosynth Res* **87**, 73–81 (2006).

6. Kaltenbrunner, M. *et al.* Ultrathin and lightweight organic solar cells with high flexibility. *Nat Commun* **3**, (2012).

7. Hou, J., Inganas, O., Friend, R. H. & Gao, F. Organic solar cells based on non-fullerene acceptors. *Nature Materials* vol. 17 119–128 Preprint at https://doi.org/10.1038/NMAT5063 (2018).

8. Janssen, R. A. J. & Nelson, J. Factors Limiting Device Efficiency in Organic Photovoltaics. *Advanced Materials* **25**, 1847–1858 (2013).

9. Sauvé, G. & Fernando, R. Beyond Fullerenes: Designing Alternative Molecular Electron Acceptors for Solution-Processable Bulk Heterojunction Organic Photovoltaics. *J Phys Chem Lett* **6**, 3770–3780 (2015).

10. Bakulin, A. A., Martyanov, D. S., Paraschuk, D. Yu., Pshenichnikov, M. S. & van Loosdrecht, P. H. M. Ultrafast Charge Photogeneration Dynamics in Ground-State Charge-Transfer Complexes Based on Conjugated Polymers. *J Phys Chem B* **112**, 13730–13737 (2008).

11. Hou, G. *et al.* Life cycle assessment of grid-connected photovoltaic power generation from crystalline silicon solar modules in China. *Appl Energy* **164**, 882–890 (2016).

12. Green, M. *et al.* Solar cell efficiency tables (version 57). *Progress in Photovoltaics: Research and Applications* **29**, 3–15 (2021).

13. Cui, Y. *et al.* Single-Junction Organic Photovoltaic Cell with 19% Efficiency. *Advanced Materials* **33**, 2102420 (2021).

14. Gao, W. *et al.* Achieving 19% Power Conversion Efficiency in Planar-Mixed Heterojunction Organic Solar Cells Using a Pseudosymmetric Electron Acceptor. *Advanced Materials* **34**, 2202089 (2022).

15. Mateker, W. R. & McGehee, M. D. Progress in Understanding Degradation Mechanisms and Improving Stability in Organic Photovoltaics. *Advanced Materials* **29**, 1603940 (2017).

16. Zhang, Y., Samuel, I. D. W., Wang, T. & Lidzey, D. G. Current Status of Outdoor Lifetime Testing of Organic Photovoltaics. *Advanced Science* **5**, 1800434 (2018).

17. Rieβ, W., Karg, S., Dyakonov, V., Meier, M. & Schwoerer, M. Electroluminescence and photovoltaic effect in PPV Schottky diodes. *J Lumin* **60–61**, 906–911 (1994).

18. Antoniadis, H., Hsieh, B. R., Abkowitz, M. A., Jenekhe, S. A. & Stolka, M. Photovoltaic and photoconductive properties of aluminum/poly(p-phenylene vinylene) interfaces. *Synth Met* **62**, 265–271 (1994).

19. Hoppe, H. & Sariciftci, N. S. Organic solar cells: An overview. *J Mater Res* **19**, 1924–1945 (2004).

20. Tang, C. W. Two-layer organic photovoltaic cell. *Appl Phys Lett* **48**, 183–185 (1986).

21. Halls, J. J. M., Pichler, K., Friend, R. H., Moratti, S. C. & Holmes, A. B. Exciton diffusion and dissociation in a poly(p-phenylenevinylene)/C60 heterojunction photovoltaic cell. *Appl Phys Lett* **68**, 3120–3122 (1996).

22. Haugeneder, A. *et al.* Exciton diffusion and dissociation in conjugated polymer/fullerene blends and heterostructures. *Phys Rev B* **59**, 15346–15351 (1999).

23. Theander, M. *et al.* Photoluminescence quenching at a polythiophene/C-60 heterojunction. *Phys Rev B* **61**, 12957–12963 (2000).

24. Stübinger, T. & Brütting, W. Exciton diffusion and optical interference in organic donor-acceptor photovoltaic cells. *J Appl Phys* **90**, 3632–3641 (2001).

25. Markov, D. E., Amsterdam, E., Blom, P. W. M., Sieval, A. B. & Hummelen, J. C. Accurate measurement of the exciton diffusion length in a conjugated polymer using a heterostructure with a side-chain cross-linked fullerene layer. *Journal of Physical Chemistry A* **109**, 5266–5274 (2005).

26. Yu, G., Nishino, H., Heeger, A. J., Chen, T.-A. & Rieke, R. D. *Enhanced electroluminescence from semiconducting polymer blends*. *Synthetic Metals* vol. 72 (1995).

27. Halls, J. J. M. *et al.* Efficient photodiodes from interpenetrating polymer networks. *Nature* **376**, 498–500 (1995).

28. Yiwen Wang. Stability of Nonfullerene Organic Solar Cells . (2019).

29. Li, N. *et al.* Abnormal strong burn-in degradation of highly efficient polymer solar cells caused by spinodal donor-acceptor demixing. *Nat Commun* **8**, 14541 (2017).

30. Speller, E. M. *et al.* From fullerene acceptors to non-fullerene acceptors: prospects and challenges in the stability of organic solar cells. *J. Mater. Chem. A* **7**, 23361–23377 (2019).

31. Cheng, P. & Zhan, X. Stability of organic solar cells: challenges and strategies. *Chem. Soc. Rev.* **45**, 2544–2582 (2016).

32. Glatthaar, M. *et al.* Efficiency limiting factors of organic bulk heterojunction solar cells identified by electrical impedance spectroscopy. *Solar Energy Materials and Solar Cells* **91**, 390–393 (2007).

33. Wang, M. *et al.* Degradation mechanism of organic solar cells with aluminum cathode. *Solar Energy Materials and Solar Cells* **95**, 3303–3310 (2011).

34. Norrman, K., Madsen, M. v, Gevorgyan, S. A. & Krebs, F. C. Degradation Patterns in Water and Oxygen of an Inverted Polymer Solar Cell. *J Am Chem Soc* **132**, 16883–16892 (2010).

35. Reese, M. O. *et al.* Photoinduced Degradation of Polymer and Polymer–Fullerene Active Layers: Experiment and Theory. *Adv Funct Mater* **20**, 3476–3483 (2010).

36. Classen, A. *et al.* Revealing Hidden UV Instabilities in Organic Solar Cells by Correlating Device and Material Stability. *Adv Energy Mater* **9**, 1902124 (2019).

37. Jeong, J. *et al.* Significant Stability Enhancement in High-Efficiency Polymer:Fullerene Bulk Heterojunction Solar Cells by Blocking Ultraviolet Photons from Solar Light. *Adv Sci (Weinh)* **3**, 1500269 (2015).

38. Patel, J. B. *et al.* Effect of Ultraviolet Radiation on Organic Photovoltaic Materials and Devices. *ACS Appl Mater Interfaces* **11**, 21543–21551 (2019).

39. Yousif, E. & Haddad, R. Photodegradation and photostabilization of polymers, especially polystyrene: review. *Springerplus* **2**, 398 (2013).

40. Rivaton, A. *et al.* Photostability of organic materials used in polymer solar cells. *Polym Int* **63**, 1335–1345 (2014).

41. Jørgensen, M., Norrman, K. & Krebs, F. C. Stability/degradation of polymer solar cells. *Solar Energy Materials and Solar Cells* **92**, 686–714 (2008).

42. Jørgensen, M., Norrman, K. & Krebs, F. C. Stability/degradation of polymer solar cells. *Solar Energy Materials and Solar Cells* **92**, 686–714 (2008).

43. Soon, Y. W. *et al.* Correlating triplet yield, singlet oxygen generation and photochemical stability in polymer/fullerene blend films. *Chemical Communications* **49**, 1291–1293 (2013).

44. Soon, Y. W. *et al.* Material crystallinity as a determinant of triplet dynamics and oxygen quenching in donor polymers for organic photovoltaic devices. *Adv Funct Mater* **24**, 1474–1482 (2014).

45. Klumbies, H. *et al.* Water ingress into and climate dependent lifetime of organic photovoltaic cells investigated by calcium corrosion tests. *Solar Energy Materials and Solar Cells* **120**, 685–690 (2014).

46. Unterleitner, F. C. & Hormats, E. I. Rates of Decay of Phosphorescence from Triphenylene in Acrylic Polymers. *J Phys Chem* **69**, 2516–2520 (1965).

47. Abdou, M. S. A., Orfino, F. P., Son, Y. & Holdcroft, S. Interaction of Oxygen with Conjugated Polymers: Charge Transfer Complex Formation with Poly(3-alkylthiophenes). *J Am Chem Soc* **119**, 4518–4524 (1997).

48. Hintz, H. *et al.* Photodegradation of P3HT−A Systematic Study of Environmental Factors. *Chemistry of Materials* **23**, 145–154 (2011).

49. Gijzeman, O. L. J., Kaufman, F. & Porter, G. Oxygen quenching of aromatic triplet states in solution. Part 1. *J. Chem. Soc., Faraday Trans. 2* **69**, 708–720 (1973).

50. Arbogast, J. W. *et al.* Photophysical properties of sixty atom carbon molecule (C60). *J Phys Chem* **95**, 11–12 (1991).

51. Ohkita, H. *et al.* Radical ion pair mediated triplet formation in polymer–fullerene blend films. *Chem. Commun.* 3939–3941 (2006) doi:10.1039/B608832E.

52. Soon, Y. W. *et al.* Correlating triplet yield, singlet oxygen generation and photochemical stability in polymer/fullerene blend films. *Chem. Commun.* **49**, 1291–1293 (2013).

53. Speller, E. M. *et al.* Toward Improved Environmental Stability of Polymer:Fullerene and Polymer:Nonfullerene Organic Solar Cells: A Common Energetic Origin of Light- and Oxygen-Induced Degradation. *ACS Energy Lett* **4**, 846–852 (2019).

54. Sudakov, I. *et al.* The Interplay of Stability between Donor and Acceptor Materials in a Fullerene-Free Bulk Heterojunction Solar Cell Blend. *Adv Energy Mater* **10**, 2002095 (2020).

55. Park, S. H. *et al.* Bulk heterojunction solar cells with internal quantum efficiency approaching 100%. *Nat Photonics* **3**, 297–302 (2009).

56. Liang, Y. *et al.* For the Bright Future—Bulk Heterojunction Polymer Solar Cells with Power Conversion Efficiency of 7.4%. *Advanced Materials* **22**, E135–E138 (2010).

57. Liao, S.-H., Jhuo, H.-J., Cheng, Y.-S. & Chen, S.-A. Fullerene Derivative-Doped Zinc Oxide Nanofilm as the Cathode of Inverted Polymer Solar Cells with Low-Bandgap Polymer (PTB7-Th) for High Performance. *Advanced Materials* **25**, 4766–4771 (2013).

58. Lee, H. K. H. *et al.* The role of fullerenes in the environmental stability of polymer:fullerene solar cells. *Energy Environ Sci* **11**, 417–428 (2018).

59. Brumboiu, I. E. *et al.* The influence of oxygen adsorption on the NEXAFS and core-level XPS spectra of the C60 derivative PCBM. *J Chem Phys* **142**, 054306 (2015).

60. Wadsworth, A. *et al.* Critical review of the molecular design progress in non-fullerene electron acceptors towards commercially viable organic solar cells. *Chemical Society Reviews* vol. 48 1596–1625 Preprint at https://doi.org/10.1039/c7cs00892a (2019).

61. Lechêne, B. P. *et al.* Organic solar cells and fully printed super-capacitors optimized for indoor light energy harvesting. *Nano Energy* **26**, 631–640 (2016).

62. Cui, Y. *et al.* Wide-gap non-fullerene acceptor enabling high-performance organic photovoltaic cells for indoor applications. *Nat Energy* **4**, 768–775 (2019).

63. Cui, Y. *et al.* 1 cm2 Organic Photovoltaic Cells for Indoor Application with over 20% Efficiency. *Advanced Materials* **31**, 1904512 (2019).

64. Lee, H. K. H. *et al.* The role of fullerenes in the environmental stability of polymer:fullerene solar cells. *Energy Environ. Sci.* **11**, 417–428 (2018).

65. Brumboiu, I. E. *et al.* The influence of oxygen adsorption on the NEXAFS and core-level XPS spectra of the C_{60} derivative PCBM. *J Chem Phys* **142**, 054306 (2015).

66. Guo, J. *et al.* Suppressing photo-oxidation of non-fullerene acceptors and their blends in organic solar cells by exploring material design and employing friendly stabilizers. *J. Mater. Chem. A* **7**, 25088–25101 (2019).

67. Uddin, A., Upama, M. B., Yi, H. & Duan, L. Encapsulation of organic and perovskite solar cells: A review. *Coatings* vol. 9 Preprint at https://doi.org/10.3390/coatings9020065 (2019).

68. Norrman, K., Larsen, N. B. & Krebs, F. C. Lifetimes of organic photovoltaics: Combining chemical and physical characterisation techniques to study degradation mechanisms. *Solar Energy Materials and Solar Cells* **90**, 2793–2814 (2006).

69. Du, X. *et al.* Efficient Polymer Solar Cells Based on Non-fullerene Acceptors with Potential Device Lifetime Approaching 10 Years. *Joule* **3**, 215–226 (2019).

70. Yu, Z.-P. *et al.* Simple non-fused electron acceptors for efficient and stable organic solar cells. *Nat Commun* **10**, 2152 (2019).

71. Wu, J. *et al.* Exceptionally low charge trapping enables highly efficient organic bulk heterojunction solar cells. *Energy Environ Sci* **13**, 2422–2430 (2020).

72. Zheng, Z. *et al.* Tandem Organic Solar Cell with 20.2% Efficiency. *Joule* **6**, 171–184 (2022).

73. He, C. *et al.* Manipulating the D:A interfacial energetics and intermolecular packing for 19.2% efficiency organic photovoltaics. *Energy Environ Sci* **15**, 2537–2544 (2022).

74. Kong, X. *et al.* 18.55% Efficiency Polymer Solar Cells Based on a Small Molecule Acceptor with Alkylthienyl Outer Side Chains and a Low-Cost Polymer Donor PTQ10. *CCS Chemistry* 1–10 (2022) doi:10.31635/ccschem.022.202202056.

75. Yuan, J. *et al.* Single-Junction Organic Solar Cell with over 15% Efficiency Using Fused-Ring Acceptor with Electron-Deficient Core. *Joule* **3**, 1140–1151 (2019).

76. Zhao, Y. *et al.* Revealing the photo-degradation mechanism of PM6:Y6 based high-efficiency organic solar cells. *J Mater Chem C Mater* **9**, 13972–13980 (2021).

77. Sun, C. *et al.* A low cost and high performance polymer donor material for polymer solar cells. *Nat Commun* **9**, (2018).

78. Zhang, M., Guo, X., Ma, W., Ade, H. & Hou, J. A Large-Bandgap Conjugated Polymer for Versatile Photovoltaic Applications with High Performance. *Advanced Materials* **27**, 4655–4660 (2015).

79. Dong, Y. *Transient Spectroscopic Studies of Charge Carrier Dynamics in Organic Solar Cells*. (2020).

80. van Amerongen, H. & van Grondelle, R. [9] Transient absorption spectroscopy in study of processes and dynamics in biology. in *Methods in Enzymology* vol. 246 201–226 (Academic Press, 1995).

81. Characteristics of Fluorescence Emission. in *Molecular Fluorescence* 53–74 (John Wiley & Sons, Ltd, 2012). doi:https://doi.org/10.1002/9783527650002.ch3.

82. Ramohlola, K. E., Iwuoha, E. I., Hato, M. J. & Modibane, K. D. Instrumental Techniques for Characterization of Molybdenum Disulphide Nanostructures. *J Anal Methods Chem* **2020**, 8896698 (2020).

83. Arif, O. *et al.* GaAs/GaP superlattice nanowires: growth, vibrational and optical properties. *Nanoscale* (2022) doi:10.1039/D2NR02350D.

84. Salmanion, M., Kondov, I., Vandichel, M., Aleshkevych, P. & Najafpour, M. M. Surprisingly Low Reactivity of Layered Manganese Oxide toward Water Oxidation in Fe/Ni-Free Electrolyte under Alkaline Conditions. *Inorg Chem* **61**, 2292–2306 (2022).

85. Hagler, T. W., Pakbaz, K., Voss, K. F. & Heeger, A. J. *Enhanced order and electronic delocalization in conjugated polymers oriented by gel processing in polyethylene*. *PHYSICAL REVIEW B* vol. 44 (1991).

86. Hagler, T. W., Pakbaz, K., Voss, K. F. & Heeger, A. J. *Enhanced order and electronic delocalization in conjugated polymers oriented by gel processing in polyethylene*. *PHYSICAL REVIEW B* vol. 44 (1991).

87. Birdwell, J. E. & Engel, A. S. Characterization of dissolved organic matter in cave and spring waters using UV–Vis absorbance and fluorescence spectroscopy. *Org Geochem* **41**, 270–280 (2010).

88. De, S. *et al.* Geminate Charge Recombination in Alternating Polyfluorene Copolymer/Fullerene Blends. *J Am Chem Soc* **129**, 8466–8472 (2007).

89. Westenhoff, S. *et al.* Charge Recombination in Organic Photovoltaic Devices with High Open-Circuit Voltages. *J Am Chem Soc* **130**, 13653–13658 (2008).

90. Clarke, T. *et al.* Transient absorption spectroscopy of charge photogeneration yields and lifetimes in a low bandgap polymer/fullerenefilm. *Chemical Communications* 91 (2008) doi:10.1039/B813815J.

91. Ohkita, H. *et al.* Radical ion pair mediated triplet formation in polymer–fullerene blend films. *Chemical Communications* 3939–3941 (2006) doi:10.1039/B608832E.

92. Westenhoff, S. *et al.* Charge Recombination in Organic Photovoltaic Devices with High Open-Circuit Voltages. *J Am Chem Soc* **130**, 13653–13658 (2008).

93. Howard, I. A. *et al.* Charge recombination and exciton annihilation reactions in conjugated polymer blends. *J Am Chem Soc* **132**, 328–335 (2010).

94. Wang, K., Chen, H., Zhang, J., Zou, Y. & Yang, Y. Intrachain and Interchain Exciton-Exciton Annihilation in Donor-Acceptor Copolymers. *Journal of Physical Chemistry Letters* **12**, 3928–3933 (2021).

95. Kraabel, B. *et al.* Unified picture of the photoexcitations in phenylene-based conjugated polymers: Universal spectral and dynamical features in subpicosecond transient absorption. *Phys Rev B* **61**, 8501–8515 (2000).

96. Yan, M., Rothberg, L. J., Kwock, E. W. & Miller, T. M. Interchain Excitations in Conjugated Polymers. *Phys Rev Lett* **75**, 1992–1995 (1995).

97. Martini, I. B., Smith, A. D. & Schwartz, B. J. Exciton-exciton annihilation and the production of interchain species in conjugated polymer films: Comparing the ultrafast stimulated emission and photoluminescence dynamics of MEH-PPV. *Phys Rev B* **69**, 35204 (2004).

98. Shoaee, S. & Durrant, J. R. Oxygen diffusion dynamics in organic semiconductor films. *J Mater Chem C Mater* **3**, 10079–10084 (2015).

99. Distler, A. *et al.* Effect of PCBM on the Photodegradation Kinetics of Polymers for Organic Photovoltaics. *Chemistry of Materials* **24**, 4397–4405 (2012).

100. Fraga Domínguez, I., Distler, A. & Lüer, L. Stability of Organic Solar Cells: The Influence of Nanostructured Carbon Materials. *Adv Energy Mater* **7**, 1601320 (2017).

101. Hoke, E. T. *et al.* The Role of Electron Affinity in Determining Whether Fullerenes Catalyze or Inhibit Photooxidation of Polymers for Solar Cells. *Adv Energy Mater* **2**, 1351–1357 (2012).

102. Nelson, J. Diffusion-limited recombination in polymer-fullerene blends and its influence on photocurrent collection. *Phys Rev B* **67**, 155209 (2003).

103. Shuttle, C. G. *et al.* Bimolecular recombination losses in polythiophene: Fullerene solar cells. *Phys Rev B* **78**, 113201 (2008).

104. Friederich, P. *et al. The influence of impurities on the charge carrier mobility of small molecule organic semiconductors*.

105. Zhang, W. *et al.* 16.52% Efficiency All-Polymer Solar Cells with High Tolerance of the Photoactive Layer Thickness. *Advanced Materials* **34**, (2022).

106. Yang, Y. *et al.* Side-Chain Isomerization on an n-type Organic Semiconductor ITIC Acceptor Makes 11.77% High Efficiency Polymer Solar Cells. *J Am Chem Soc* **138**, 15011–15018 (2016).

107. Manceau, M. *et al.* Photochemical stability of π-conjugated polymers for polymer solar cells: A rule of thumb. *J Mater Chem* **21**, 4132–4141 (2011).

108. Guo, Y. *et al.* Synthesis of a Low-Cost Thiophene-Indoloquinoxaline Polymer Donor and Its Application to Polymer Solar Cells. *Polymers (Basel)* **14**, (2022).

109. Alem, S. *et al.* Degradation mechanism of benzodithiophene-based conjugated polymers when exposed to light in air. *ACS Appl Mater Interfaces* **4**, 2993–2998 (2012).

110. Du, J. *et al.* Polymerized small molecular acceptor based all-polymer solar cells with an efficiency of 16.16% via tuning polymer blend morphology by molecular design. *Nat Commun* **12**, 5264 (2021).

111. Wang, X. *et al.* Simple Nonfused Ring Electron Acceptors with 3D Network Packing Structure Boosting the Efficiency of Organic Solar Cells to 15.44%. *Adv Energy Mater* **11**, 2102591 (2021).

112. Yang, C. *et al.* Molecular design of a non-fullerene acceptor enables a P3HT-based organic solar cell with 9.46% efficiency. *Energy Environ Sci* **13**, 2864–2869 (2020).

113. Griffini, G., Turri, S. & Levi, M. Degradation and stabilization of poly(3-hexylthiophene) thin films for photovoltaic applications. *Polymer Bulletin* **66**, 211–222 (2011).

114. Posada, F., Philippart, J.-L., Kappler, P. & Gardette, J.-L. Photooxidation of cured fluorinated polymers—I. Photooxidation of copolymers of fluorinated olefins and allyl or vinyl ethers. *Polym Degrad Stab* **50**, 141–158 (1995).

115. Manceau, M., Rivaton, A. & Gardette, J.-L. Photochemical Stability of Materials for OPV. in *Stability and Degradation of Organic and Polymer Solar Cells* 71–108 (2012). doi:https://doi.org/10.1002/9781119942436.ch4.

116. Hintz, H. *et al.* Photodegradation of P3HT−A Systematic Study of Environmental Factors. *Chemistry of Materials* **23**, 145–154 (2011).

117. He, Z. *et al.* Enhanced power-conversion efficiency in polymer solar cells using an inverted device structure. *Nat Photonics* **6**, 591–595 (2012).

118. Razzell-Hollis, J. *et al.* Photochemical stability of high efficiency PTB7:PC70BM solar cell blends. *J Mater Chem A Mater* **2**, 20189–20195 (2014).

119. Rech, J. J. *et al.* Designing Simple Conjugated Polymers for Scalable and Efficient Organic Solar Cells. *ChemSusChem* **14**, 3561–3568 (2021).

120. Li, X. *et al.* Simplified synthetic routes for low cost and high photovoltaic performance n-type organic semiconductor acceptors. *Nat Commun* **10**, 519 (2019).

121. Dang, M. T., Hirsch, L. & Wantz, G. P3HT:PCBM, Best Seller in Polymer Photovoltaic Research. *Advanced Materials* **23**, 3597–3602 (2011).

122. Zhou, K. *et al.* Unraveling the Correlations between Mechanical Properties, Miscibility, and Film Microstructure in All-Polymer Photovoltaic Cells. *Adv Funct Mater* (2022) doi:10.1002/adfm.202201781.